Testing the use of single- and multi-mission satellite altimetry for the calibration of hydraulic models

# Testing the use of single- and multi-mission satellite altimetry for the calibration of hydraulic models

Alessio Domeneghetti [(1)], Giada Molari[(1)], Mohammad J. Tourian[(2)], Angelica Tarpanelli[(3)], Sajedeh Behnia[(2)], Tommaso Moramarco[(3)], Nico Sneeuw[(2)], Armando Brath[(1)]

[(1)]*Department DICAM, University of Bologna, Bologna, Italy*

*Email: alessio.domeneghetti@unibo.it; giada.molari@unibo.it; armando.brath@unibo.it*

[(2)] *Institute of Geodesy, University of Stuttgart, Germany,*

*Email: tourian@gis.uni-stuttgart.de; sajedeh.behnia@gis.uni-stuttgart.de; sneeuw@gis.uni-stuttgart.de*

[(3)] *Research Institute for Geo-Hydrological Protection, National Research Council, Perugia, Italy*

*Email: angelica.tarpanelli@irpi.cnr.it; tommaso.moramarco@irpi.cnr.it*

## HIGHLIGHTS

- Comparison of available altimetry products for hydrodynamic model calibration
- Investigation of the potential of multi-mission series for calibrating hydraulic model
- Impact of single- and multi-mission series length (n° of observations) on calibration reliability
- Results show the improvement of satellite performances over time
- Multi-mission series outperform short series of original low-frequency altimetric products

**ABSTRACT**

Satellite altimetry is increasingly considered as a valuable source of information in many hydrological and hydraulic applications. However, the accuracy of different sensors adopted for monitoring the water level from satellite and the limited temporal resolution that characterizes each sensor (i.e. revisit time most of time varying from 10 to 35 days; 369 days in case of CryoSat mission) still hamper their common use. Recently introduced multi-mission (MM) densified time series might represent a possible alternative to ensure higher spatial and temporal coverage. Though, a comparison of the potential of different altimetry products, including MM series, for hydrodynamic model calibration is still missing. This study attempts to fill this gap investigating how available altimetry series perform over a stretch of the Po River (nearly 140 km across Northern Italy) in calibrating a quasi-2D model built with detailed topographic information. Specifically, objectives are manifold: i) to provide a comparison of satellite altimetry products available to the research community and commonly used in hydraulic modelling (Envisat, Envisat extended mission, ERS-2, TOPEX/Poseidon, SARAL/AltiKa, Jason-2, Jason-3, Sentinel 3A, Sentinel 3B and CryoSat); ii) to evaluate the performance of MM satellite series in calibrating a hydraulic model relative to single-mission series; and iii) to investigate the importance of the number of observations (series length) for each mission.

Results of the model calibration depict a general improvement of satellite performance over time, moving from the oldest to more recent missions, with the exception of Envisat extended series. In general, Jason-2, Sentinel 3A and Sentinel 3B outperform other series both in terms of calibration error and number of measurements required to achieve a reliable calibration. MM series provide errors larger than those obtained from original single-mission time series considered with their overall length, but they provide more reliable calibrations than altimetric time series with low sampling rate (i.e., Envisat, Envisat extended, and SARAL/AltiKa) or those that cover very short periods (e.g. altimetry series limited to 20-40 months in length). The analysis offers additional insights into the possible use of altimetry series in hydrodynamic applications, providing a comparison of different original products and showing the potential, as well as limitations, offered by MM series.

**KEYWORDS:**

Remote sensing, Satellite altimetry, Hydraulic model calibration, Uncertainty analysis, Po river.

## 1 INTRODUCTION

Over the last thirty years hydraulic modelling has developed to such an extent that it can now provide high-quality flood risk maps (Merz *et al*., 2010), damage assessment (Luino *et al*., 2009), water resource management (Loucks *et al*., 2005), real-time flood forecasting (Arduino *et al*., 2005) and dynamic perspective in case of future scenarios (Bronstert, 2003). Hydraulic modelling describes the flood routing and, hence, tracks the propagation of a flood wave given as an input at an upstream location of a river channel to any downstream locations. The routing model requires an accurate geometric description of the river channel and floodplains, reliable input of river discharge and the calibration of the roughness parameter, considered as the most important factor that has an impact on predicting flow characteristics (Aronica *et al*., 1998; Bates *et al*., 1996; Pappenberger *et al*., 2005). The model calibration generally consists in tuning the roughness parameter to minimize the misfit between simulated and observed output represented by flow or water level hydrographs. Typically, the calibration is done by using water level or discharge observations gathered at the gauged stations available along the river. Recently, scientific literature is enriched by studies on the integration of remote sensing and ground observations for hydraulic model calibration. Numerous examples use the flood extent derived by the backscatter value of Synthetic Aperture Radar (SAR) images to calibrate the roughness parameter (Andreadis *et al*., 2014; Schumann *et al*., 2014; Wood *et al*., 2016; Matgen *et al*., 2011; Tarpanelli *et al*., 2013a), in some cases considering also the uncertainty in the flood extraction (Di Baldassarre *et al*., 2009; Giustarini *et al*., 2015). Directly related to the water surface elevation, satellite altimetry has demonstrated its large potential in the calibration of 1D or 2D hydraulic models (Domeneghetti *et al*., 2014, O'Loughlin *et al*., 2013; Yan *et al*., 2014). Neal *et al*. (2012) calibrated the hydraulic model LISFLOOD-FP for an 800 km reach of the Niger river in Mali using the laser altimetry data from Ice, Cloud, and land Elevation Satellite, ICESat. Differently from the radar altimetry data that are collected with a given repeat period at the same locations, ICESat does not produce repeat-track measurements and, although considered the most accurate source of altimetry information, the hydrological community is still sceptical about monitoring rivers in a different way from the traditional adoption of fixed gauging stations (O'Loughlin *et al*., 2016). Similarly, CryoSat-2 satellite suffers from a limited use due to the almost annual repeat cycle (i.e., 369 days), which is considered inadequate to represent river dynamics. However, its dense spatial sampling (about 7.5 km at the equator) can be extremely useful in deriving water level profiles that normally cannot be achieved. Schneider

*et al*. (2018) used CryoSat-2 water level data to calibrate the Manning roughness coefficient each 10 km over the Po river main channel by using the DHI Mike 11 software (DHI, 2015). Compared with values calibrated through in situ measurements, CryoSat-2 showed a strong potential to calibrate the roughness coefficient at a more detailed level with the consequent reduction of the over- and under-estimation of the high flows (Jiang *et al*., 2019).

Concerning traditional radar altimetry (i.e. short-repeat and fixed-orbit missions, such as ERS-2, Envisat, and Jason-2), several examples have demonstrated its valid contribution in supporting the ground network for describing the hydrometric regime (Garambois *et al*., 2017; Emery *et al*., 2016) and the potential benefits expected in case of its integration with in situ data (Domeneghetti *et al*., 2014; Huang *et al*., 2018 and reference therein). Similar studies have mostly focused on rivers larger in width than about 300 m, a limitation imposed by the along-track spatial resolution of delay/Doppler altimetry. The Fully Focused SAR (FF-SAR) processing, however, improves the along-track resolution of SAR altimetry up to the theoretical threshold of half of the antenna length (Egido and Smith, 2016; Vignudelli *et al*., 2019). Kleinherenbrink *et al*. (2020) have implemented the FF-SAR algorithm over lakes, canals, and ditches in Netherlands using CryoSat-2 full-bit-rate data. For cases where the altimetry track crosses the water bodies in a near-perpendicular angle, they have successfully derived the water level of a ditch as small as 5 m in width and located only 10 m away from a canal. Though more studies are required to indicate the potentials and limitations of FF-SAR, it is expected that the method would open an unprecedented opportunity to monitor smaller water bodies. Moreover, when the future SWOT mission is fully operational, for rivers wider than 100 m (possibly as narrow as 50 meters; Desai, 2018; Frasson *et al.*, 2019), a 2D river mapping at 10-70 m resolution is anticipated (Biancamaria *et al*., 2016). Concerning the use of traditional radar altimetry for the calibration of the hydraulic model, two limitations are the most relevant and worth to be analysed: the length (duration) of the time series and the revisit time of the satellite.

The importance of the duration (i.e., years of observation or number of overpasses) of the satellite mission has been analysed by Domeneghetti *et al*. (2015) who showed its impact on the estimation of the roughness coefficient. In particular, they found that sample sizes of 2.5 years can be considered sufficient to the calibration process in case of using ERS-2 and Envisat time series. However, an extension of similar investigations to other satellites is desirable to assess the potential of current and past altimetry missions for

hydraulic simulations.

Also, the revisit time, typically 10 to 35 days for altimetry missions, represents a limitation for hydrodynamic applications. A possible solution is the development of approaches that consider the use of multiple missions (MM) to derive densified time series in specific locations. Tourian *et al*. (2016) transferred the water level information coming from four satellite missions (Jason-2, Envisat, SARAL and CryoSat-2) and, hence, several virtual stations, to specific locations of the river coincident with the ground monitoring stations along the Po, Mississippi, Congo and Danube rivers. The combination of the altimetry data has been carried out with the hydraulic concepts of wave travel time and celerity of the flow calculated with the geometric characteristics of the river, such as length of the reach, slope and width. A successive study of Tourian *et al*. (2017) analysed a similar approach over the Niger river and obtained river discharge by assimilating altimetric and in situ river discharge with a Kalman filter approach. Boergens *et al*. (2017) integrated water level measurements of Envisat, SARAL and Jason-2 by using ordinary kriging in the main channel of the Mekong River. All these attempts to increase the frequency of sampling of the river water surface are valuable contributions especially for hydrological applications and for deriving more frequent discharge time series. However, the value of MM time series has never been tested in hydraulic modelling.

Moving from previous considerations, the present work proposes to investigate three main aspects that are still only partially analysed in the literature:

1) to compare the available altimetry data in terms of their performance for the calibration of hydraulic models. Specifically, the analysis provides a comprehensive comparison of different satellite altimetry products available to the research community and covering nearly 27 years, such as: Envisat (E), Envisat extended mission (EX), TOPEX/Poseidon (TP), SARAL/AltiKa (SA), Jason-2 (J2) and Jason-3 (J3), Sentinel 3A (S3A) and Sentinel 3B (S3B). Despite not directly analysed, the potential of ERS-2 and CryoSat is also presented taking advantage of previous studies carried out on the same study area (Domeneghetti *et al*., 2015; Schneider *et al*., 2018);
2) to assess the effect of the record length (i.e., number of available satellite measurements, in relation to different data products) on the calibration reliability. The study investigates the possible accuracy of the model calibration in relation to the record length of the altimetry product adopted for its execution. This info could be beneficial not only at the early stages of a mission, but also when historical time

series are limited in length (perhaps due to missing values or mission interruption). Findings of such evaluation might serve a modeller when called to evaluate the extent of the calibration period;

3) to test the use of MM satellite time series in the process of hydraulic model calibration. These synthetic altimetry time series result from the combination of different single-mission time series and overcome the spatial and temporal sampling limits that characterize a given single mission (see e.g., Tourian *et al*., 2016).

The construction of MM time series represents a recent frontier towards a larger exploitation of altimetry data provided from the overall set of past and on-going satellite missions (see also Coss et al., 2020). Thus, the evaluation of its potential for the implementation of an accurate and reliable hydraulic model constitutes an element of interest for the hydrologic community. Although not claiming to provide a general statement and ranking of the altimetry products, which would require considering a large set of rivers having a variety of hydrological and morphological characteristics, this study aims at delivering a comprehensive and cross-missions view of the potential of current and past altimetry data.

The analysis is implemented along the Po river in the stretch between the gauged stations of Borgoforte (basin area equal to 62.450 km²) and Pontelagoscuro (basin area equal to 70.091 $km^2$), for a direct comparison with other studies. The hydraulic simulation is carried out with the HEC-RAS software package (Hydrologic Engineering Center, 2001) in a quasi-2D configuration (see Section 3.1).

# 1 STUDY AREA AND ALTIMETRY TIME SERIES

## 1.1 Study area

Figure 1 presents the area of interest: about 140-km reach of the lower portion of the Po river, the largest and longest Italian river that flows in Eastern direction across Northern Italy. Considering the social and economic importance of this area, the Po river is consistently monitored and controlled by the Po River Basin Authority (AdB-Po), which records and provides hydrological and geometrical ground observations used in this study (Montanari *et al.*, 2017). The analysis focuses on the river reach that is limited upstream by the gauging station of Borgoforte and downstream by the beginning of the river delta. Along this portion, the main channel width ranges from 200 to 500 m, while lateral floodplains may span up to 2.5 km.

Figure 1 shows Virtual Stations, VSs (locations where satellite tracks cross with the river), considered in this

study, as well as the position of gauged stations (i.e., Borgoforte and Pontelagoscuro) where river discharge and water surface elevation are recorded daily from 1923 and 1922, respectively. Although Po river dynamic and its off seasonal behaviour may result challenging for the use of altimetry data, it represents a profitable case study where both traditionally observed and remotely sensed hydrological data are available (Domeneghetti *et al*., 2014, 2015).

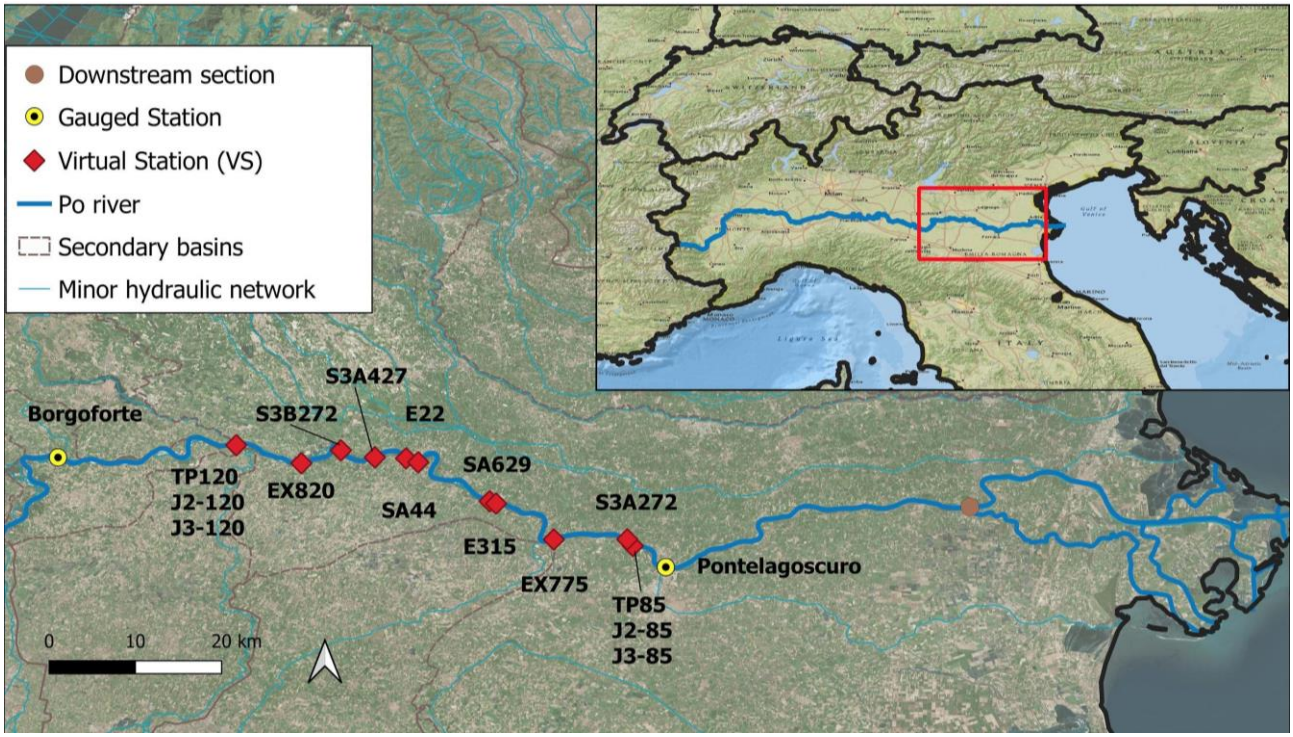


***Figure 1***. *Po river stretch considered in the study (140 km, from Borgoforte to the beginning of the river delta) with the identification of gauged stations and the virtual stations (VSs) relative to the overall set of satellite missions.*

### 1.2 Satellite altimetry products

Table 1 summarizes the different altimetry missions considered in the study: Envisat (E), Envisat Extended Mission (EX), TOPEX/Poseidon (TP), SARAL/AltiKa (SA), Jason-2 (J2), Jason-3 (J3), Sentinel-3A (S3A) and Sentinel-3B (S3B). These missions are characterized by different sensors instrumentation, scopes, and orbits. Therefore, the respective altimetry time series are characterized by distinctive temporal and spatial resolution as well as different accuracy and reliability. Most of the considered missions have a low temporal resolution (i.e. 35 days for E and SA, 30 days for EX, and 27 days for S3A and S3B), while TP, J2 and J3 provide water surface elevation measurements every 10 days. E (mission period 05/2002–10/2010) and SA (03/2013–01/2016) are the successors of the former mission ERS-2 (04/1995–09/2007) using the same orbit

configuration with inter-track distance of 80 km at equator and a repeat cycle of 35 days. E, EX, and SA data are processed adopting ICE-1 retracker, shown to provide robust and accurate results over rivers (Frappart *et al*., 2006; Silva *et al*., 2010). J2, launched in June 2008, is the successor of the former missions TP (09/1992–08/2002), and J3 was launched in 2016 as the successor of J2 and placed in the same orbit with the inter-track distance of about 315 km at equator and a repeat cycle of 10 days. For both J2 and J3, the water levels are derived using the ICE retracker, as it has proven to outperform other retrackers over continental waters (Cretaux, J. F. *et al*., 2018). The currently active S3A and S3B guarantee the continuity of E-type measurements in a fully operational manner. Sentinel-3 provides SAR altimetry data with a revisit time of 27 days. The two missions have orbits almost similar to that of E and ERS, with the ground-track separation of 104 km at equator. S3A and S3B data are processed using the OCOG retracker which is a heritage of ICE-1, and hence, reliable for inland applications.

All water level time series are processed using the high-rate altimetry datasets. The usual rate for all missions is 20 Hz which leads to the along-track distance of 294 m between successive measurements. SA dataset however is provided with the sampling rate of 40 Hz, and hence, the spatial spacing of 173 m along-track. For clarity, Figure 2 presents the temporal coverage of the altimetry products considered in the study, while Figure 3 reports a synoptic view of the water levels derived from the different missions.

***Table 1***. *Satellite sensors and altimetry time series considered in this study.*

| ***Mission (Abbreviation)*** | ***Version*** | ***Retracker*** | ***Observation period*** | ***Temporal resolution [day]*** | ***Height [km]*** | ***Inclination [degree]*** | ***Data source*** |
|---|---|---|---|---|---|---|---|
| TOPEX/Poseidon (TP) | MGDR-B | onboard | 1992–2002 | 9.91 | 1336 | 66 | PODAAC |
| Envisat (E) | GDR-V3 | ICE-1 | 2002–2010 | 35 | 800 | 98.5 | ESA |
| Envisat XT (EX) | GDR-V3 | ICE-1 | 2010–2012 | 35 | 800 | 98.5 | ESA |
| SARAL/AltiKa (SA) | GDR-t | ICE-1 | 2013–2016 | 35 | 800 | 98.5 | AVISO |
| JASON 2 (J2) | PISTACH | ICE-3 | 2008–2015 | 9.91 | 1336 | 66 | AVISO |
| JASON 3 (J3) | GDR-d | ICE | 2016-2019 | 10 | 1336 | 66 | AVISO |
| Sentinel-3A (S3A) | O_NT_003 | OCOG | 2016-2019 | 27 | 814.5 | 95.65 | COPERNICUS |
| Sentinel-3B (S3B) | O_NT_003 | OCOG | 2018-2019 | 27 | 814.5 | 95.65 | COPERNICUS |
| Multi-mission (MM) | | | 1995–2019 | ca. 3 | | | - |

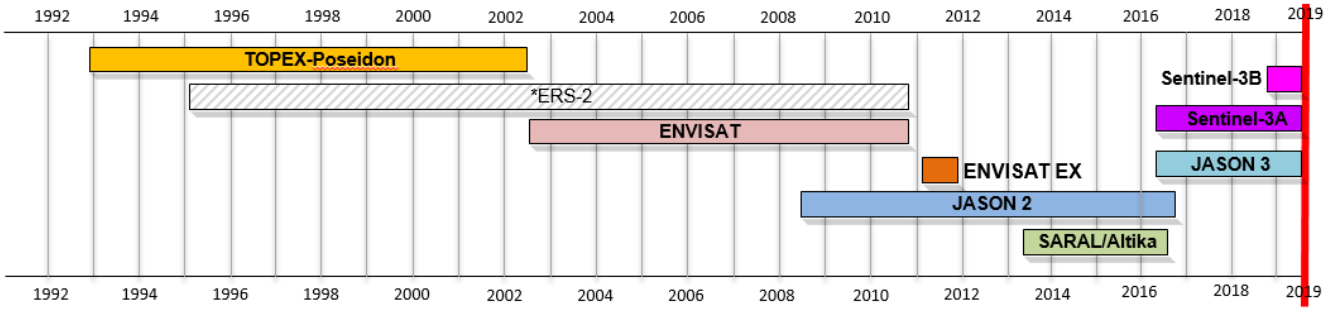


***Figure 2**. Temporal distribution of satellite altimetry missions used in this work: TOPEX/Poseidon, Envisat, Envisat EX, JASON-2, SARAL/AltiKa, JASON-3, Sentinel-3A, and Sentinel-3B (*ERS-2 is reported for comparison with other studies in literature).*

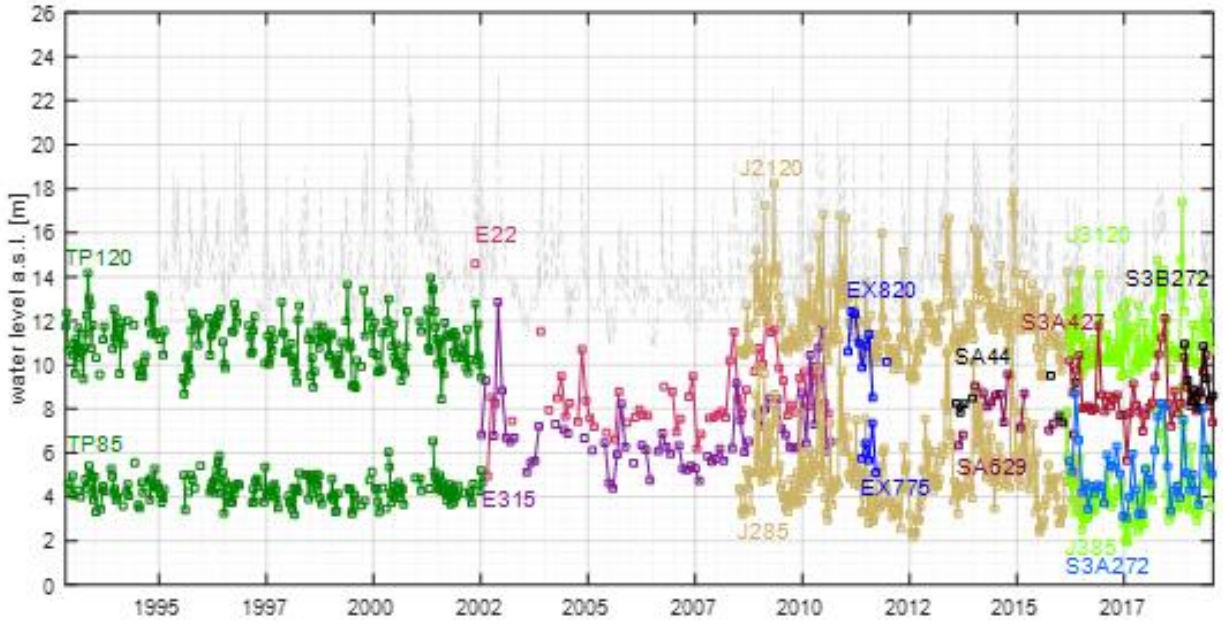


***Figure 3**. Synoptic view of altimetry time series at VSs identified along the river stretch of interest. The grey dashed line reports water levels observed at Borgoforte.*

Referring to the same study area, Tarpanelli *et al.* (2013b) and Domeneghetti *et al.*, (2014, 2015) investigated the potential of ERS-2 time series for similar purposes. The comparison of ERS-2 with water level values recorded at the nearest gauging station, or estimated at VSs, shows significant correlations, with the mean absolute error in the order of 0.7 m. In particular, Domeneghetti *et al.*, (2015) investigated the effect of ERS-2 uncertainty on model calibration, while Schneider *et al*., (2018) did the same considering CryoSat time series. For the sake of brevity, and to avoid the repetition of already performed investigations, calibrations with ERS-2 and CryoSat data are not carried out in this work. Actually, the drifting orbit of CryoSat implies a long-repeat ground track pattern that would impose the adoption of different calibration strategies (i.e., it is not straightforward to construct time series since its long repeat cycle – 369 day). Nevertheless, this does affect

the completeness of this investigation: results previously obtained with both ERS-2 and CryoSat are summarized and compared with those of other altimetry time series to provide a complete overview of altimetry performance.

### 1.3 Multi-mission (MM): altimetry time series at high spatial and temporal coverage

Water level time series from individual altimetry missions over the river are merged using an approach developed by Tourian *et al*. (2016) to overcome spatial and temporal limitation of single altimetry missions. Adopting this solution all VSs of several satellite altimeters along the Po River are connected to each other hydraulically and statistically. To this end, first the bias between different missions is removed (see Tourian *et al*., 2016, for more details). Then, for any given location along the river, the time lag due to stream flow between the altimetric virtual stations and the selected location is estimated. Since the MM approach has been developed for being applicable also on poorly surveyed areas, average river width using imagery together with the slope derived from satellite altimetry are used as inputs to a simple empirical hydraulic equation that estimates average flow velocity and thus the time lag between VSs (Bjerklie *et al*., 2005; Tourian *et al*., 2015). Figure 4 shows the estimated time lag between VS along the Po River highlighted with those selected for this study. From the most upstream selected VS in this study (TP120, J2-120 and J3-120; see Figure 1) till most downstream VS (TP85, J2-85 and J3-85), the time lag is about 0.85 day.

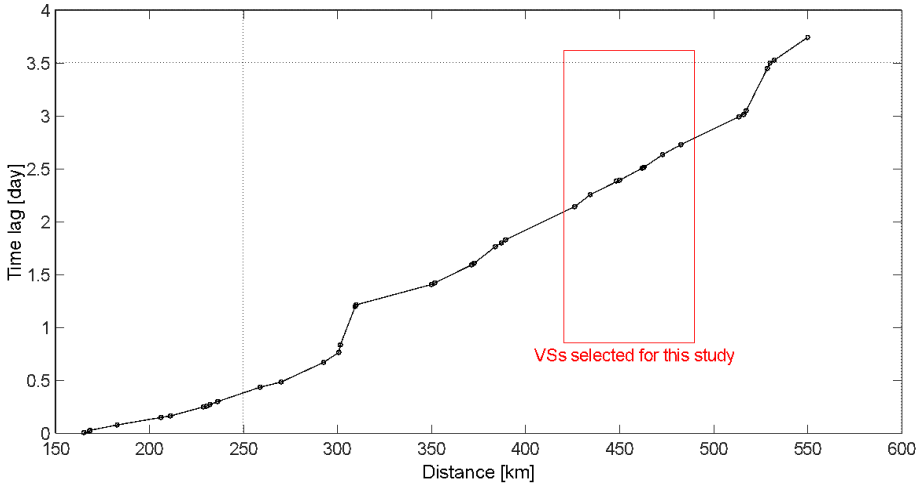


***Figure 4.*** *Estimated time lag between each VS along the Po River relative to the very first VS. The red box highlights VSs selected for this study (from Tourian et al., 2016).*

Using the estimated time lag, the water level hydrographs of all measurements are shifted and stacked at the

selected location. The stacked time series at the selected location is then normalized according to its statistical distribution and especially the water level value at 3rd and 85th percentiles as lower and upper bounds. As an example, Figure 5 shows normalized water level obtained at VS J2-85, for which first the time lag between all VSs and the J2-85 is corrected and then individual time series are normalized according to their 3rd and 85th percentiles.

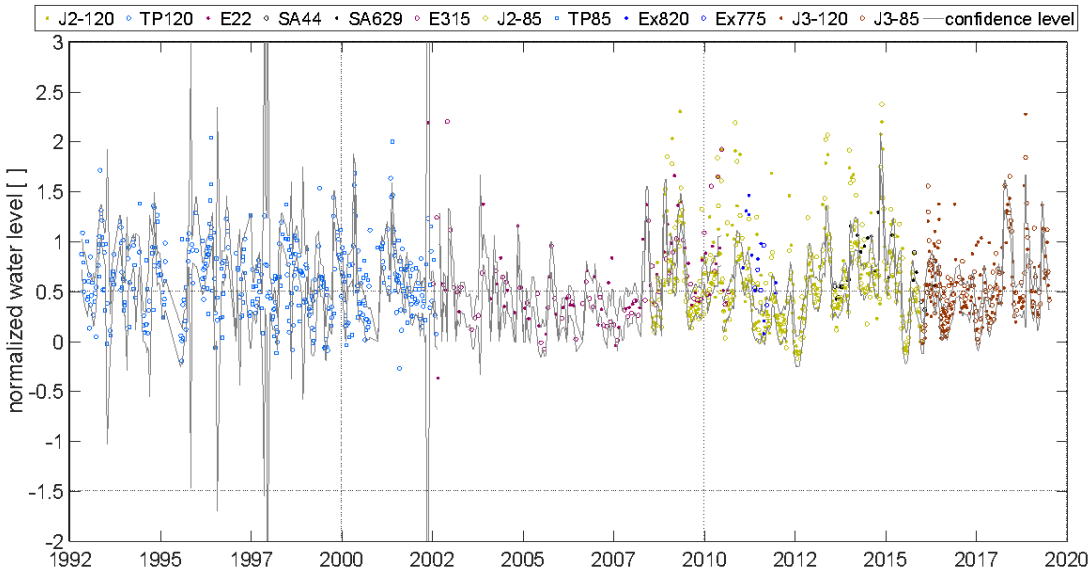


***Figure 5.*** *Normalized water level values at VS J2-85. The gray curves show the boundaries of confidence limit after rejecting all possible outliers.*

Afterwards, outliers are identified and removed from the normalized time series by defining a confidence limit of 99% of a Student's t test for a one month sliding time window. The confidence limit is delineated in Figure 5 by an upper- and a lower bound confidence level. All measurements outside the confidence limit are identified as outlier and removed from measurements. The outlier-free normalized time series is then rescaled back according to the water level distribution of the selected location (Figure 6).

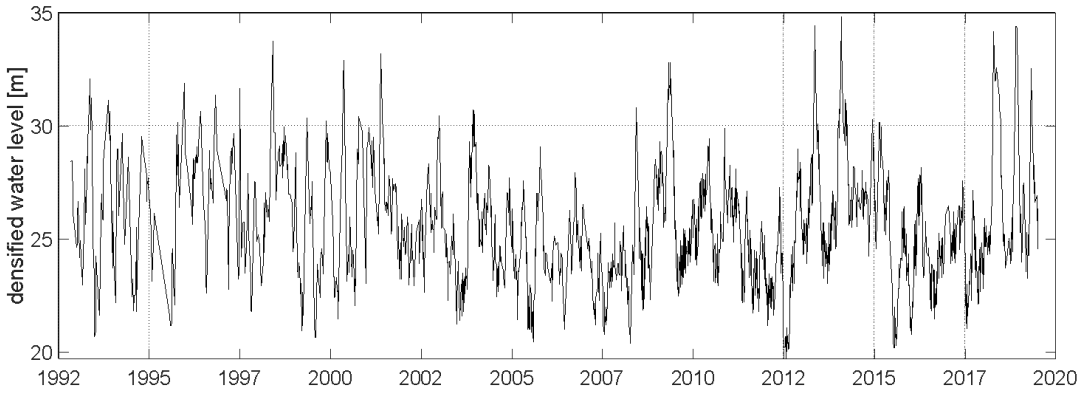


***Figure 6**. Densified water level time series at VS J2-85*

Using this methodology, we obtain a time series with 3 days effective temporal resolution from altimetry missions originally with temporal resolution ranging from 10 to 35 days.

The MM water level time series are validated at the gauging stations of Borgoforte and Pontelagoscuro, for which individual water level time series are densified, obtaining correlation coefficient equal to 0.75 and 0.78, RMSE (root mean square error) of the value of 0.94 m and 0.75 m, and bias of 0.05 and 0.37 m, respectively.

The accuracy of MM series inevitably conveys the simplifications and assumptions of the approach used for their construction. Thought for applications in data scarce areas, those simplifications mainly regards the description of the river geometry and dynamics (i.e., river width and time lag). Investigating the impacts of such limitations on the use of MM series for the calibration was out of the scope of this work. Nevertheless, these analyses are suggested for future work.

## 2 NUMERICAL ANALYSIS AND METHODOLOGICAL APPROACH

### 2.1 Model set-up, calibration and validation

The numerical simulations of the river stretch of interest is carried out by means of a quasi-two-dimensional (quasi-2D) model implemented with the HEC-RAS code that uses an implicit four-point finite difference algorithm to solve the De Saint-Venant equations. The river geometry is properly reproduced by taking advantage of a 2-m DEM (Digital Elevation Model) available along the overall Po river, which combines a LiDAR survey of the emerged river portion with traditional ground cross-sections and multi-beam sonar surveys (Camorani *et al.*, 2006). The quasi-2D scheme ensures a proper representation of the flow dynamics by enabling mutual interactions between the main channel and a series of lateral floodplains (i.e. storage areas)

delimited by a system of minor dikes, which are schematized within the code as lateral structures. Although the numerical scheme refers to 1D hydraulic equations, the adoption of this schematization enables a proper simulation of the hydraulic interaction among the main channel and lateral floodplains. The appropriateness of this configuration has been proven by a number of previous studies that referred to the same river portion (Castellarin *et al.*, 2011; Castellarin *et al.*, 2011a; Domeneghetti *et al.*, 2015).

The numerical simulations for the overall period of interest (1992-2019) are carried out by imposing the mean daily discharge values recorded at the upstream gauged station (Borgoforte) as upstream boundary conditions, and the normal flow condition at the downstream cross-section located at the beginning of the river delta (see Figure 1). According to previous experiences on the study area (Domeneghetti *et al*., 2014, 2015a), lateral inflows of some minor tributaries are not taken into account during the simulation since their contributions are neglectable relative to the Po river discharge.

The calibration procedure focuses on the identification of the Manning coefficient, $n$ ($s \cdot m^{-1/3}$), of the main channel that maximizes the Nash-Sutcliffe efficiency (NS; Nash and Sutcliffe, 1970) coefficient obtained in reproducing the observed water levels, by varying it within the range 0.01-0.06 $s \cdot m^{-1/3}$. Because the quasi-2D model has limited sensitivity to the roughness coefficient adopted for the floodplains, its value is considered constant and equal to 0.1 $s \cdot m^{-1/3}$ for all the numerical simulations (see also Castellarin *et al.*, 2011a; Domeneghetti *et al.*, 2015a).

Referring to the simulation time frame considered in this study (1995-2019), calibration and validation schemes vary in relation to investigation setting, as indicated hereafter:

a) analysis considering one VS at time, referring separately to the dataset retrieved from specific altimetry mission (Table 1, Figure 1) and the MM time series. In each calibration, the roughness coefficient is unique and assumed to be static through time. For each single mission the calibration is performed referring to the overall period of altimetry data availability (see Figure 3); once calibrated, the model validation is carried out comparing simulated water surface levels with in situ data available within the considered time frame (1995-2019) and not used for the calibration. For a single MM series that covers the overall period of interest, the latter is split in two parts: 1995-2017 for calibration, 2017-2019 for validation.

b) Analysis considering all MM time series together: the calibration adopts spatially distributed parameterization by splitting the river into a number of stretches corresponding to VSs locations and

302 considering multiple roughness coefficients.

303 When referring to MM time series, the calibration covers the period that consider the presence of all altimetry
304 missions. Its considerable extent (22 years, from 1995 to 2017) ensures a data series length sufficient to ensure
305 a consolidated calibration, guaranteeing at the same time a sufficient validation period (2 years, 2018-2019).

306

307 ### 2.2 Accuracy of altimetry products

308 Typically, as spotted in Figure 1, VSs do not coincide with gauging stations and thus a direct comparison
309 between traditional observation and remotely sensed data is not straightforward. To overcome this problem we
310 compare the satellite-derived water surface elevation values, $h_{sat}(x,t)$, sensed at a given location, $x$, at the
311 day of the satellite overpass, $t$, with the in situ water surface elevation, $h_{situ}(x,t)$, linearly interpolated at the
312 track location referring to concurrent water levels measured at the gauging stations located upstream and
313 downstream the satellite track. This appears reasonable in the absence of diversion structures or dams along
314 the river portion of interest. Following this approach, the error, $\varepsilon(x,t)$, can be calculated with the equation (1):

$$\varepsilon(x,t) = h_{sat}(x,t) - h_{situ}(x,t) \quad (1)$$

315

316 which has been applied distinguishing all the altimetry products.

317 The same approach is used considering the MM time series, where *t* covers all days of observation sensed by
318 at least one of the considered altimetry missions.

319 Considering that different altimetry missions use different reference ellipsoids (TOPEX ellipsoid for TP, J2,
320 J3, and SA, and the WGS84 for E, EX, S3A, and S3B), we calculate the geoid height with respect to the one
321 adopted for MM creation (EGM2008). The same for in situ data, which refer to ITALGEO 2005 geoid
322 (Barzaghi *et al*., 2007).

323

324 ### 2.3 Impact of VS time series length on calibration

325 The length of an altimetry dataset, *m* (i.e., the number of satellite overpasses available at a given VS
326 from a specific altimeter, which differs from the official mission duration), influences the reliability of the
327 calibration (Domeneghetti *et al.*, 2015a). To investigate its impact for different satellite products we repeat the
328 calibration exercise by considering several altimetry subsets randomly sampled from each original altimetry

time series (i.e., E, TP, J2, etc.) with a length $m$ that varies from 3 to $L_{tot}$. In this case, $L_{tot}$ indicates the total amount of altimetric observations available for a given mission at a specific VS. Indicating with $x$ the location of a given VS along the study area, the subset sampled from the original altimetry time series and used for the calibration can be expressed as:

$$h_{sat,m}(x) = [h_{sat}(x, t_1), \dots, h_{sat}(x, t_m)] \quad \forall m = 3, \dots, L_{tot} \tag{2}$$

For $m$ lower than 3, the time series is considered too short and not suitable for calibration purposes. To overcome the uncertainty related to the selection of the $m$ observations among those available for a given mission, and at a given VS, the sampling procedure is embedded in a Monte Carlo framework that generates 1000 random $h_{sat,m}$ samples for each $m$ value. Once sampled, the calibration is carried out considering each $h_{sat,m}$ sample at time.

Finally, with the aim to infer the error introduced by the altimetry data, we repeat the same procedure by calibrating the numerical model with reference to different subsets randomly extracted from the water level values observed in situ at the VS ($h_{situ}$). Eq. (3) indicates the in situ time series randomly extracted from the overall set:

$$h_{situ,m}(x) = [h_{situ}(x, t_1), \dots, h_{situ}(x, t_m)] \quad \forall m = 3, \dots, L_{tot} \tag{3}$$

Calibration results obtained with these $h_{situ,m}(x)$ samples are used as a reference for evaluating the potential of altimetry for model calibration.

For what regards the adoption of MM time series, in order to make the calibration performances of MM and traditional time series comparable, we refer to specific observation periods instead of considering a given number of observations ($m$). The observation period is expressed in terms of a number of months from the date of the first altimetry observation and varies in relation to the revisit time of each mission: 12 months for TP, J2, and J3 (i.e., high-frequency missions), 14 months for S3A and 20 months for other missions. Based on this temporal discretization, once identified a given observation period (e.g., 1, 2, …, $n$ observation periods), the number of altimetry observations adopted for the calibration for both MM and traditional time series is defined as the sum of all available water levels values observed since the beginning of the time series.

# 3 RESULTS

## 3.1 Accuracy of altimetry products

Table 2 summarizes the results of the comparison between altimetry time series and in situ water surface elevations estimated at VS locations. In particular, the table reports the number of observations that constitutes each time series, the correlation coefficient (R) between altimetry and in situ data, the NS value, the mean absolute error (MAE) as well as the mean (μ) and standard deviation (σ) of the errors expressed following eq. (1). Altimetry products are listed in a chronological order following Figure 2. In case of VSs observed from multiple sensors (e.g. VS 85 and VS 120) each time series is considered separately.

***Table 2**. Comparison of satellite altimetry and in situ water surface levels: distance from upstream cross-section, n° of satellite data ($L_{tot}$), correlation coefficient (R ), Nash-Sutcliffe (NS), Mean Absolute Error (MAE), error mean (μ) and standard deviation (σ).*

| VS | distance [km] | n° data, $L_{tot}$ | R | NS | MAE [m] | μ [m] | σ [m] |
|---|---|---|---|---|---|---|---|
| *TP120* | 25.44 | 174 | 0.77 | 0.37 | 0.67 | -0.42 | 0.75 |
| *J2-120* | 25.44 | 298 | 0.98 | 0.93 | 0.29 | 0.18 | 0.38 |
| *J3-120* | 25.44 | 107 | 0.87 | 0.69 | 0.38 | 0.20 | 0.76 |
| *EX820* | 34.23 | 12 | 0.91 | 0.68 | 0.52 | 0.5 | 0.57 |
| *S3B272* | 42.24 | 14 | 0.96 | 0.93 | 0.25 | 0.00 | 0.32 |
| *S3A427* | 48.73 | 51 | 0.94 | 0.84 | 0.43 | 0.30 | 0.47 |
| *E22* | 49.60 | 61 | 0.85 | 0.72 | 0.34 | 0.05 | 0.87 |
| *SA44* | 50.89 | 8 | 0.92 | 0.41 | 0.46 | 0.14 | 0.55 |
| *SA629* | 65.84 | 15 | 0.96 | 0.72 | 0.44 | 0.4 | 0.3 |
| *E315* | 66.87 | 65 | 0.97 | 0.89 | 0.37 | 0.3 | 0.43 |
| *EX775* | 78.72 | 5 | -0.35 | -3.97 | 1.17 | 1.17 | 1.4 |
| *S3A272* | 86.76 | 51 | 0.96 | 0.65 | 0.88 | 0.84 | 0.50 |
| *TP85* | 88.11 | 158 | 0.6 | -0.35 | 0.54 | 0.08 | 0.7 |
| *J2-85* | 88.11 | 294 | 0.98 | 0.94 | 0.29 | 0.20 | 0.37 |
| *J3-85* | 88.11 | 99 | 0.95 | 0.86 | 0.40 | 0.24 | 0.45 |

Table 3 reports the same error statistics referring to MM time series, which is unique for each VS.

***Table 3**. Comparison of MM time series and in situ water surface levels: correlation coefficient (R ), Nash-Sutcliffe (NS), Mean Absolute Error (MAE), error mean (μ) and standard deviation (σ).*

| VS | n° data, $L_{tot}$ | R | NS | MAE [m] | μ [m] | σ [m] |
|---|---|---|---|---|---|---|
| *MM120* | 1739 | 0.81 | 0.39 | 0.88 | 0.73 | 0.81 |
| *MM820* | 1739 | 0.82 | 0.60 | 0.49 | 0.01 | 0.72 |
| *MMB272* | 1739 | 0.82 | 0.61 | 0.55 | 0.22 | 0.73 |
| *MM427* | 1739 | 0.82 | 0.49 | 0.70 | 0.51 | 0.74 |
| *MM22* | 1738 | 0.81 | 0.67 | 0.59 | 0.17 | 0.79 |
| *MM44* | 1738 | 0.81 | 0.67 | 0.58 | 0.11 | 0.79 |
| *MM629* | 1733 | 0.79 | 0.59 | 0.66 | 0.30 | 0.83 |
| *MM315* | 1734 | 0.79 | 0.58 | 0.67 | 0.32 | 0.83 |
| *MM775* | 1731 | 0.76 | 0.20 | 1.11 | 0.94 | 0.95 |
| *MMA272* | 1731 | 0.73 | -0.11 | 1.42 | 1.29 | 1.05 |
| *MM85* | 1731 | 0.73 | 0.36 | 0.90 | 0.59 | 0.98 |

### 3.2 Performance of different altimetry time series on model calibration

Table 4 summarizes the results of the model calibrations and validations carried out using each altimetry time series at a time. It reports NS, RMSE and MAE obtained at each satellite track considering the overall available

datasets, which means $m = L_{tot}$. These performance statistics are compared with the ones obtained by repeating the calibration considering in situ water level elevation interpolated at the same location, and time, of the satellite overpasses (values in brackets). Δ-RMSE and Δ-MAE quantify the additional calibration errors due to the use of altimetry data instead of in situ ones, while the last three columns report the results of the validation performed using satellite time series.

***Table 4***. *Calibration and validation results: Nash-Sutcliffe efficiency value (NS), root mean square error (RMSE) and mean absolute error (MAE) obtained adopting the overall dataset of satellite and in situ (in brackets) time series ($m = L_{tot}$).*

| | ***Calibration with Satellite (In situ) time series*** | | | ***Δ = Sat – Situ*** | | ***Validation Satellite time series*** | | |
|---|---|---|---|---|---|---|---|---|
| **VS** | **NS [-]** | **RMSE [m]** | **MAE [m]** | **Δ-RMSE [m]** | **Δ-MAE [m]** | **NS [-]** | **RMSE [m]** | **MAE [m]** |
| *TP120* | 0.52 (0.92) | 0.75 (0.32) | 0.55 (0.27) | 0.43 | 0.28 | 0.94 | 0.43 | 0.37 |
| *J2-120* | 0.93 (0.99) | 0.44 (0.14) | 0.31 (0.11) | 0.30 | 0.20 | 0.97 | 0.30 | 0.24 |
| *J3-120* | 0.61 (0.93) | 0.87 (0.39) | 0.53 (0.24) | 0.48 | 0.29 | 0.98 | 0.28 | 0.22 |
| *EX820* | 0.79 (0.99) | 0.61 (0.10) | 0.52 (0.08) | 0.51 | 0.44 | 0.95 | 0.44 | 0.34 |
| *S3B272* | 0.93 (0.99) | 0.24 (0.08) | 0.18 (0.07) | 0.16 | 0.11 | 0.62 | 1.10 | 1.04 |
| *S3A427* | 0.86 (0.97) | 0.47 (0.20) | 0.33 (0.14) | 0.27 | 0.19 | 0.95 | 0.37 | 0.26 |
| *E22* | 0.74 (0.96) | 0.83 (0.25) | 0.39 (0.20) | 0.58 | 0.19 | 0.94 | 0.42 | 0.33 |
| *SA44* | -0.08 (0.96) | 0.72 (0.23) | 0.56 (0.20) | 0.49 | 0.36 | 0.96 | 0.34 | 0.26 |
| *SA629* | 0.90 (0.97) | 0.29 (0.17) | 0.25 (0.16) | 0.12 | 0.09 | 0.87 | 0.58 | 0.48 |
| *E315* | 0.92 (0.99) | 0.46 (0.20) | 0.29 (0.15) | 0.26 | 0.14 | 0.85 | 0.63 | 0.52 |
| *EX775* | -2.95 (0.91) | 1.53 (0.22) | 1.29 (0.20) | 1.31 | 1.09 | 0.54 | 1.28 | 1.11 |
| *S3A272* | 0.91 (0.97) | 0.43 (0.22) | 0.31 (0.18) | 0.21 | 0.13 | 0.70 | 1.02 | 0.89 |
| *TP85* | -0.73 (0.80) | 0.79 (0.39) | 0.64 (0.31) | 0.40 | 0.33 | 0.82 | 0.66 | 0.42 |
| *J2-85* | 0.93 (0.98) | 0.45 (0.24) | 0.32 (0.17) | 0.21 | 0.15 | 0.78 | 0.76 | 0.52 |
| *J3-85* | 0.82 (0.92) | 0.58 (0.34) | 0.44 (0.24) | 0.24 | 0.20 | 0.80 | 0.75 | 0.52 |

Figure 7 reports the results of the calibration exercise performed considering altimetry time series of different length and randomly sampled from the original datasets (see eq. (2)). Considering each altimetry product and VS at time, panels of Figure 7 show the calibrated roughness coefficient in relation to the number of

observations, *m*, used for the calibration. The solid line indicates the Manning coefficient that ensures the optimal NS value among the 1000 calibrations performed with a given *m* value, while the grey area represents the range of variability of the roughness coefficients calibrated within the Monte Carlo framework. The wider this area, the more the results of a calibration process depend on the altimetry record used for the calibration, with the risk of being significantly influenced by the range of water levels sensed during a specific period (e.g., mainly high flows or low flows).

401

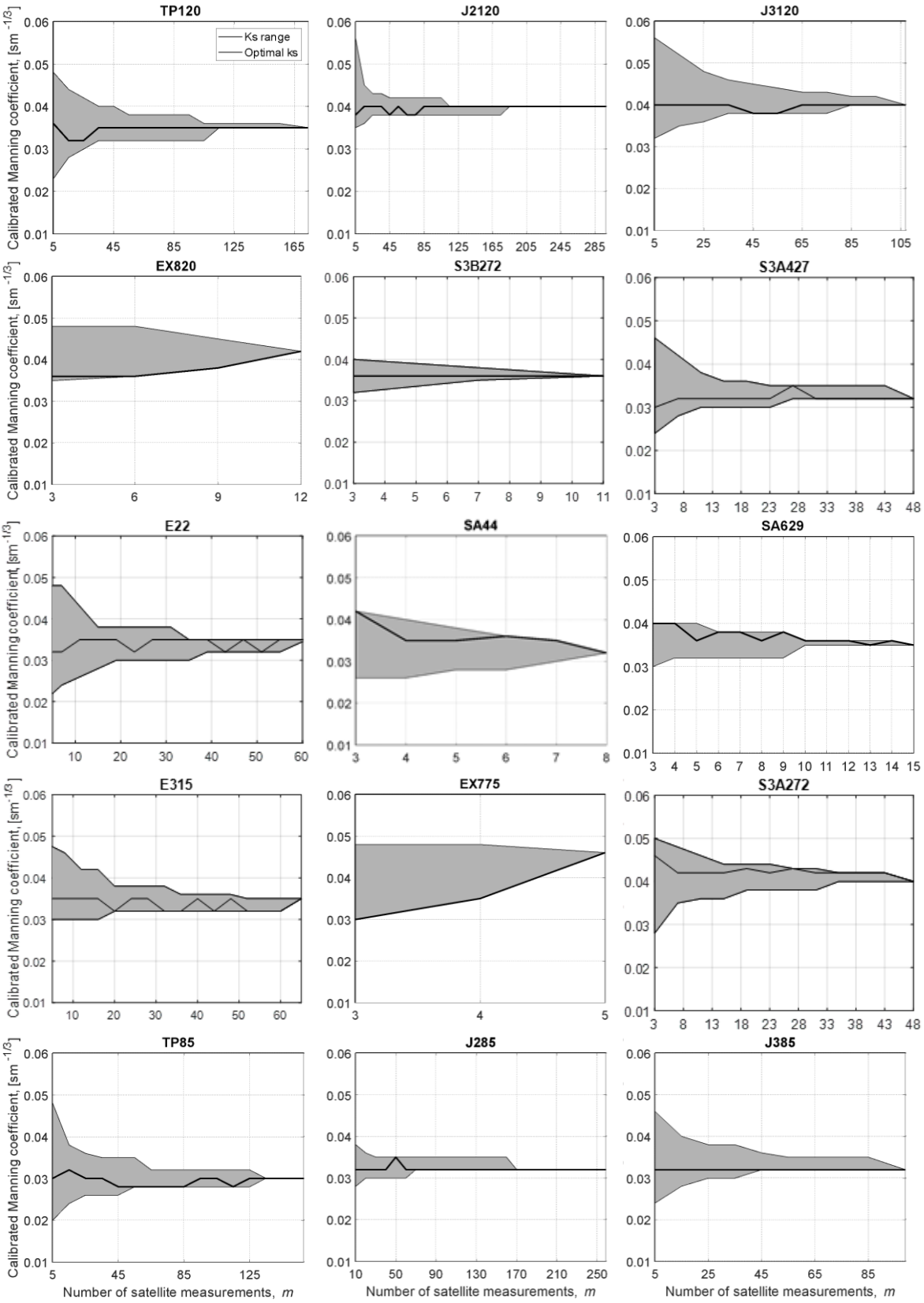
TP120
J2120
J3120
EX820
S3B272
S3A427
E22
SA44
SA629
E315
EX775
S3A272
TP85
J285
J385
Ks range
Optimal ks
Calibrated Manning coefficient, [sm^-1/3]
Number of satellite measurements, m

402

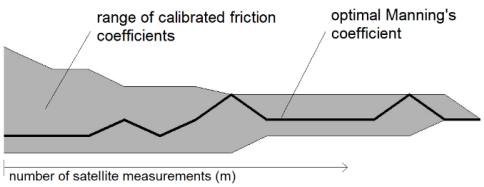


***Figure** 7. Calibration results for different altimetry series length: range of calibrated roughness coefficient (grey areas) and optimal Manning's value (black line) as a function of the number of satellite measurements, m.*

Figure 8 provides an overview of the maximum error that we can expect when we use altimetry data for the calibration of a hydrodynamic model. The black line indicates the maximum MAE as function of *m*, thus the maximum error obtained considering all possible calibrated configurations obtained in the Monte Carlo framework with a given data length (i.e., grey areas in Figure 7). The comparison with the same maximum MAE obtained calibrating the model with in situ data (red line) provides a quantitative estimation of the additional error induced by satellite altimetry uncertainty.

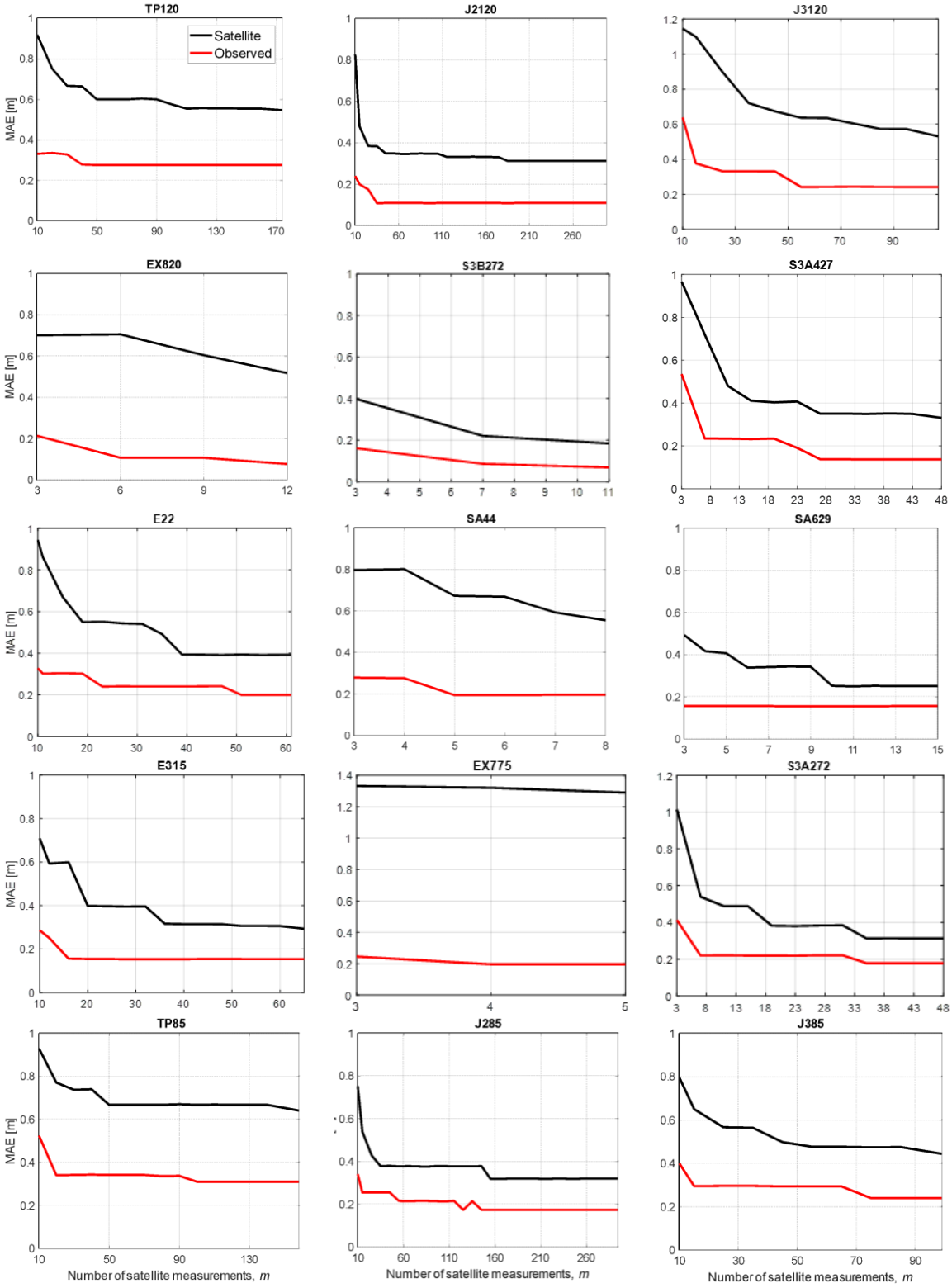


***Figure 8.*** *MAE obtained calibrating the numerical model with satellite altimetry data (black line) and in situ water levels (red line) as a function of data length, m.*

Figure 9 summarizes the findings of Figure 8 showing the temporal evolution of the performance of satellite altimetry for model calibration. The length of each box represents the temporal coverage of the mission, while

the box height identifies the range of variability of the MAE obtained during the calibration considering the overall amount of available observations (see also Table 4). In order to give a complete overview, Figure 9 also includes the results from the previous investigation using ERS-2 (see Domeneghetti *et al*., 2015a). A similar calibration exercise over the Po river was done by Schneider *et al*. (2018) using CryoSat-2 series observed during the period 2010-2016. Their findings report an average RMSE (ME, mean error) of nearly 0.4 m (-0.18 m) for the SAR mode, with values ranging from 0.06 m (-0.05 m) up to 0.63 m (-0.23 m) (not shown in Figure 9 due to the use of different error metrics).

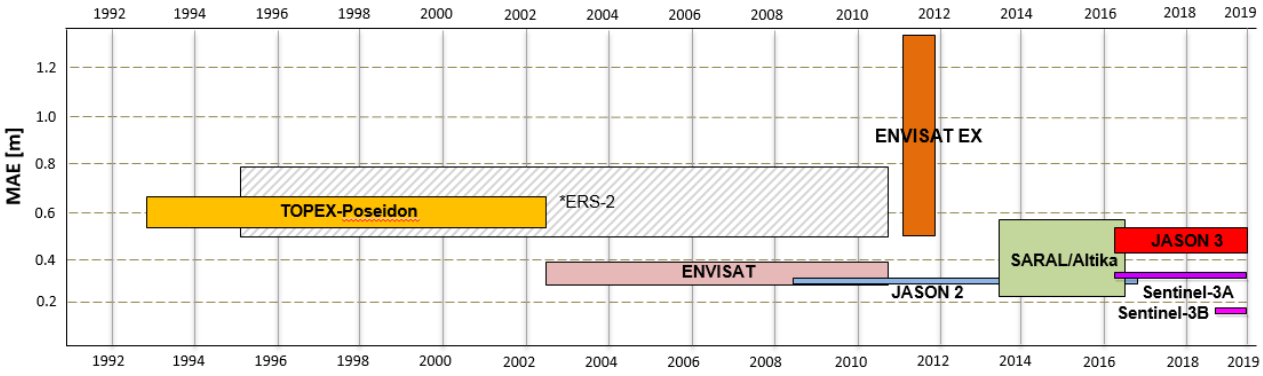


***Figure 9***. *Synoptic view of the MAE of each satellite mission in time (*ERS-2 is a recall from a previous investigation): the vertical height of each box is defined as the range of the MAE obtained from the calibration at different VSs considering* $m = L_{tot}$.

### 3.3 Performances of MM series on model calibration

Table 5 summarizes the results of the calibration (1995-2017) performed using MM series, as well as those obtained using in situ water levels observed, in the same period, at the same day of the satellite overpasses. MM series are specified for each VS sensed along the study area, thus Table 5 has only 11 rows, according to the number of intersections between the Po river and the considered satellite orbits (VSs).

***Table 5***. *Calibration and validation results: NS, RMSE and MAE obtained from the calibration process performed adopting MM and in situ (in brackets) time series ($m = L_{tot}$).*

| | ***Calibration with MM (In situ) series*** | | | ***Δ = Sat – Situ*** | | ***Validation with MM series*** | | |
|---|---|---|---|---|---|---|---|---|
| **VS** | **NS [-]** | **RMSE [m]** | **MAE [m]** | **Δ-RMSE [m]** | **Δ-MAE [m]** | **NS [-]** | **RMSE [m]** | **MAE [m]** |
| *MM120* | 0.54 (0.95) | 0.89 (0.28) | 0.64 (0.21) | 0.61 | 0.43 | 0.88 | 0.66 | 0.54 |
| *MM820* | 0.45 (0.95) | 0.80 (0.29) | 0.56 (0.22) | 0.51 | 0.34 | 0.95 | 0.39 | 0.29 |
| *MMB272* | 0.51 (0.97) | 0.80 (0.20) | 0.56 (0.13) | 0.60 | 0.43 | 0.97 | 0.28 | 0.15 |
| *MMA427* | 0.45 (0.97) | 0.78 (0.18) | 0.55 (0.13) | 0.60 | 0.42 | 0.89 | 0.54 | 0.48 |
| *MM22* | 0.63 (0.92) | 0.80 (0.33) | 0.58 (0.24) | 0.47 | 0.34 | 0.94 | 0.41 | 0.31 |
| *MM44* | 0.63 (0.93) | 0.80 (0.33) | 0.58 (0.24) | 0.47 | 0.34 | 0.93 | 0.42 | 0.31 |
| *MM629* | 0.66 (0.89) | 0.80 (0.41) | 0.58 (0.26) | 0.39 | 0.32 | 0.90 | 0.46 | 0.31 |
| *MM315* | 0.66 (0.95) | 0.76 (0.28) | 0.55 (0.19) | 0.48 | 0.19 | 0.87 | 0.56 | 0.42 |
| *MM775* | 0.65 (0.79) | 0.83 (0.58) | 0.59 (0.37) | 0.25 | 0.22 | 0.61 | 1.1 | 0.92 |
| *MMA272* | 0.65 (0.76) | 0.89 (0.63) | 0.64 (0.39) | 0.26 | 0.25 | 0.53 | 1.18 | 1.12 |
| *MM85* | 0.66 (0.72) | 0.79 (0.68) | 0.57 (0.42) | 0.11 | 0.15 | 0.70 | 0.91 | 0.67 |

As previously shown for the original satellite altimetry data (see section 3.2), Figure 10 reports the results of the calibration carried out adopting MM altimetry series of different length and randomly sampled from the datasets used for calibration. Considering each VS at a time, panels in Figure 10 show the Manning coefficient calibrated in relation to the series length, *m*. The solid black line indicates the roughness coefficient that ensures the optimal NS value among those tested for a given *m* value, while the grey area represents the range of variability of the calibrated coefficients. Even in this case, the width of the grey area is indicative of the sensibility of the calibration result to the length of the altimetry record used for the calibration. It is worth noting here that the temporal interval considered for calibration (1995-2017) is long enough to guarantee the achievement of a consolidated and stable calibration.

Figure 11 reports the maximum error obtained by calibrating the model with MM series: the black line indicates the maximum MAE as function of *m*, which is compared with the error obtained when calibrating the same model with an in situ data record of the same length (red line).

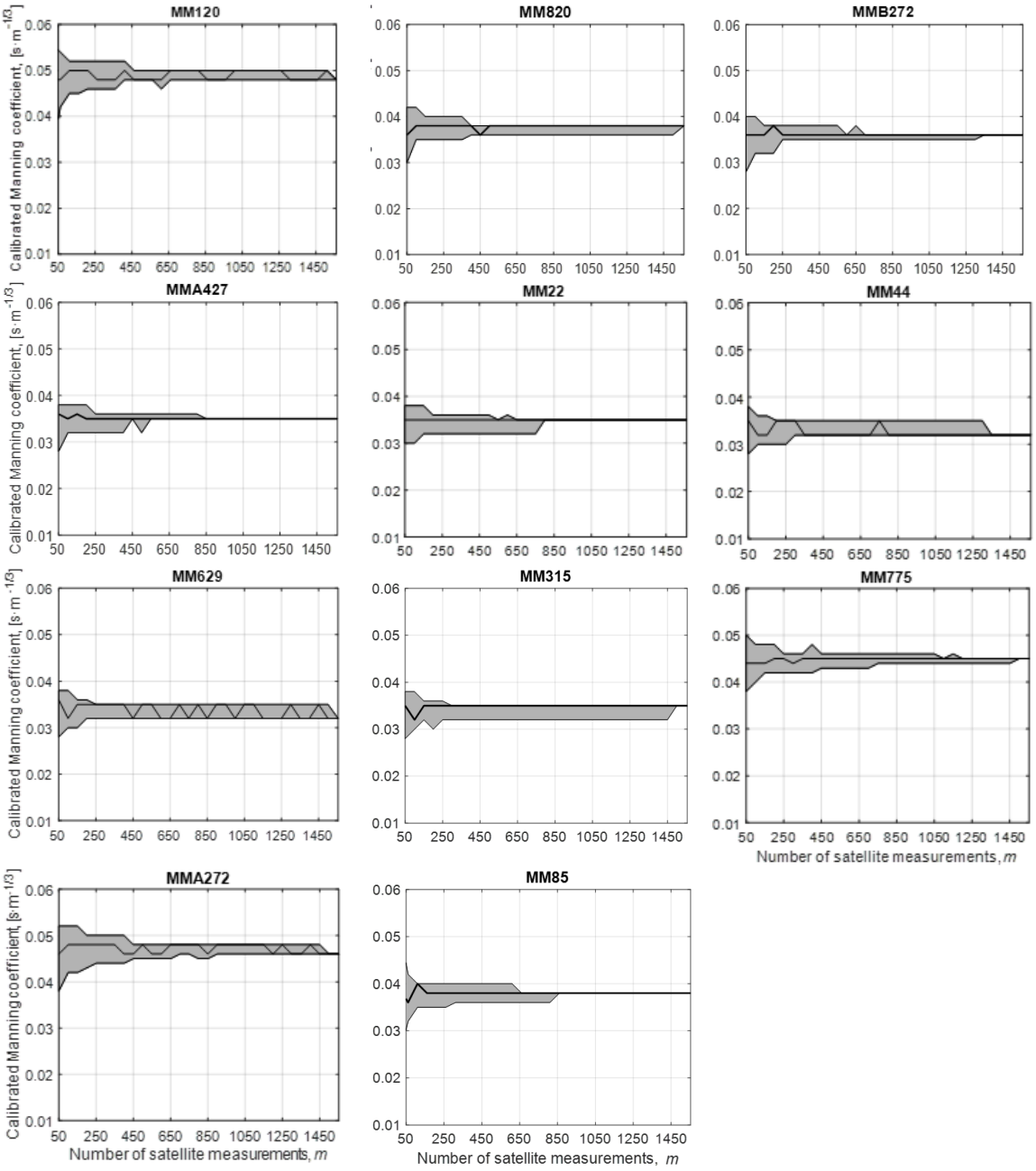


***Figure 10**. Calibration results for different MM series length: range of calibrated roughness coefficient (grey areas) and optimal Manning's value (black line) as a function of data length, m.*

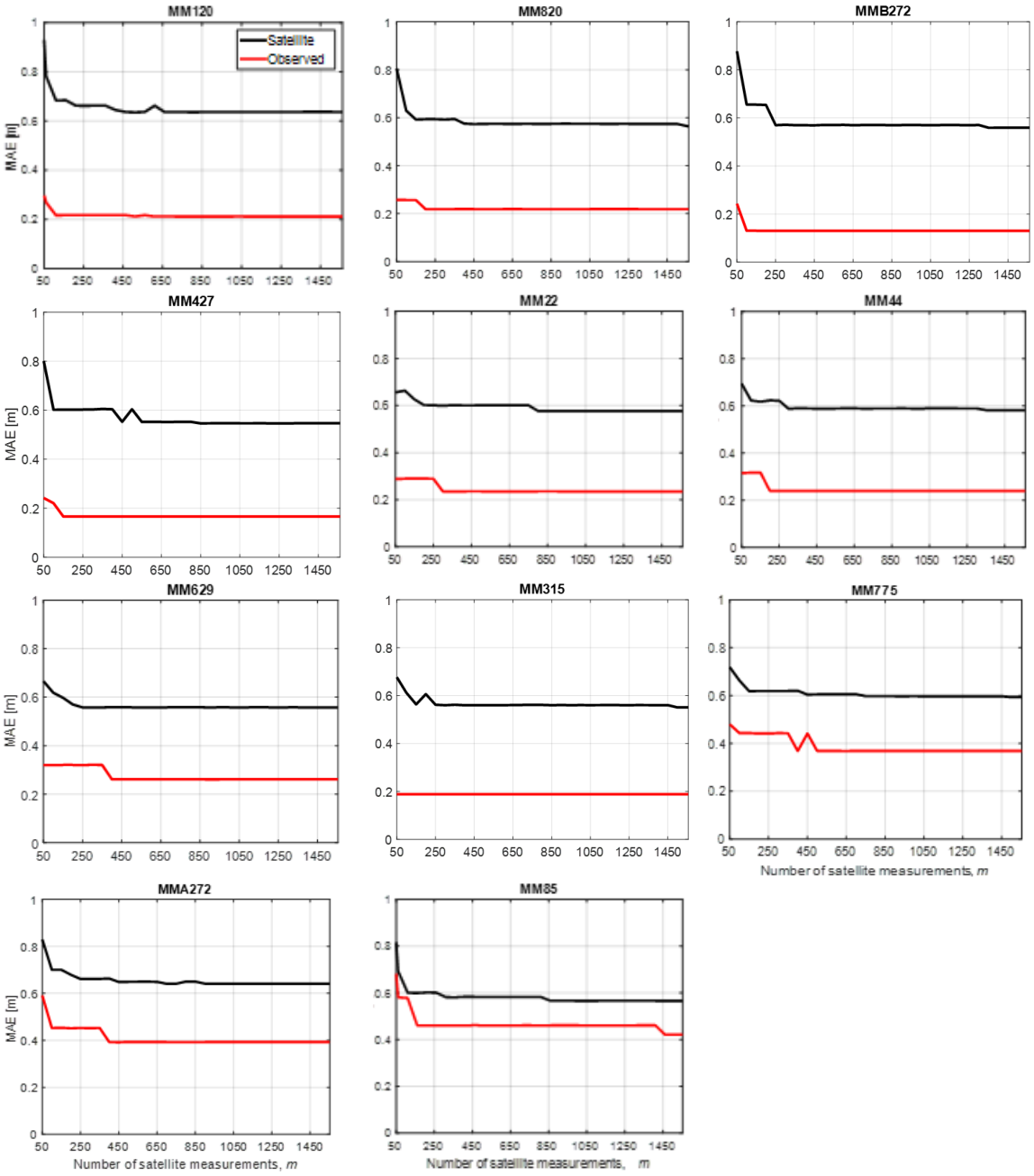


***Figure 11***. *MAE obtained calibrating the numerical model with MM altimetry data (black line) and in situ water levels (red line) as a function of data length, m.*

### 3.4 Comparison of single and MM altimetry series

Table 6 presents the calibration results obtained using the MM time series. Results are compared with those achieved by calibrating the model with the original satellite altimetry available at the different VSs. Values reported in Table 6 refer to the case of considering the overall altimetry series length ($m = L_{tot}$). Last four columns report the calibration (validation) performances when considering the overall set of MM series along the Po river.

Figures 12-17 show the comparison between original satellite series and MM ones. Each figure represents one satellite mission, E22, J2-85, SA629, TP120, J3-85 and S3A-272 from Figure 12 to 17, respectively (S3B-272 is not shown since the limited amount of data). For each figure panel a) represents the number of measurements using MM series (grey columns) and unique sensor (black columns) considering different observation periods (temporal step equal to 20 months for E22 and SA44, 2 months for J2-85, J3-85 and TP120, 14 months for S3A-272). Panels b), c) and d) depict MAE, NS variability and Manning's coefficient as a function of the number of available data, respectively.

***Table 6****. Calibration and validation results: optimal calibrated Manning's coefficient (n), and errors obtained adopting single and MM altimetry series ($m = L_{tot}$), as well as all MM series together (validation results are in brackets).*

| | **Single Orig. series** | **Single MM series** | ***Δ = MM – Orig.*** | | | **Calibration (validation) results with all MM series** | | | |
|---|---|---|---|---|---|---|---|---|---|
| **VS** | **n [$m^{1/3}s^{-1}$]** | **n [$m^{1/3}s^{-1}$]** | **Δn [$m^{1/3}s^{-1}$]** | **Δ-RMSE [m]** | **Δ-MAE [m]** | **n [$m^{1/3}s^{-1}$]** | **NSE [-]** | **RMSE [m]** | **MAE [m]** |
| *MM-TP120* | 0.035 | 0.048 | 0.013 | 0.14 | 0.09 | 0.048 | 0.39 (0.40) | 1.01 (1.06) | 0.80 (0.78) |
| *MM-J2-120* | 0.040 | 0.048 | 0.008 | 0.45 | 0.33 | | | | |
| *MM-J3-120* | 0.040 | 0.048 | 0.008 | 0.02 | 0.11 | | | | |
| *MM-EX820* | 0.042 | 0.038 | -0.004 | 0.19 | 0.04 | 0.045 | 0.53 (0.80) | 0.81 (0.60) | 0.55 (0.41) |
| *MM-B272* | 0.036 | 0.036 | / | 0.56 | 0.38 | 0.042 | 0.56 (0.59) | 0.80 (0.68) | 0.55 (0.48) |
| *MM-A427* | 0.032 | 0.035 | 0.003 | 0.31 | 0.22 | 0.04 | 0.58 (0.78) | 0.80 (0.63) | 0.55 (0.44) |
| *MM-E22* | 0.035 | 0.035 | / | -0.003 | 0.19 | 0.036 | 0.62 (0.75) | 0.80 (0.70) | 0.56 (0.50) |
| *MM-SA44* | 0.032 | 0.032 | / | 0.08 | 0.02 | 0.033 | 0.61 (0.75) | 0.81 (0.69) | 0.57 (0.50) |
| *MM-SA629* | 0.035 | 0.032 | -0.003 | 0.51 | 0.33 | 0.03 | 0.46 (0.54) | 0.96 (0.91) | 0.73 (0.69) |
| *MM-E315* | 0.035 | 0.035 | / | 0.30 | 0.26 | 0.03 | 0.44 (0.53) | 0.98 (0.93) | 0.76 (0.70) |
| *MM-EX775* | 0.046 | 0.045 | -0.001 | -0.70 | -0.70 | 0.044 | 0.54 (0.52) | 0.87 (0.90) | 0.65 (0.62) |
| *MM-A272* | 0.040 | 0.046 | 0.006 | 0.46 | 0.33 | 0.046 | 0.26 (0.11) | 1.17 (1.22) | 0.95 (0.96) |
| *MM-TP85* | 0.030 | 0.038 | 0.008 | / | -0.07 | 0.044 | 0.59 (0.63) | 0.79 (0.78) | 0.58 (0.53) |
| *MM-J2-85* | 0.032 | 0.038 | 0.006 | 0.34 | 0.25 | | | | |
| *MM-J3-85* | 0.032 | 0.038 | 0.006 | 0.21 | 0.13 | | | | |

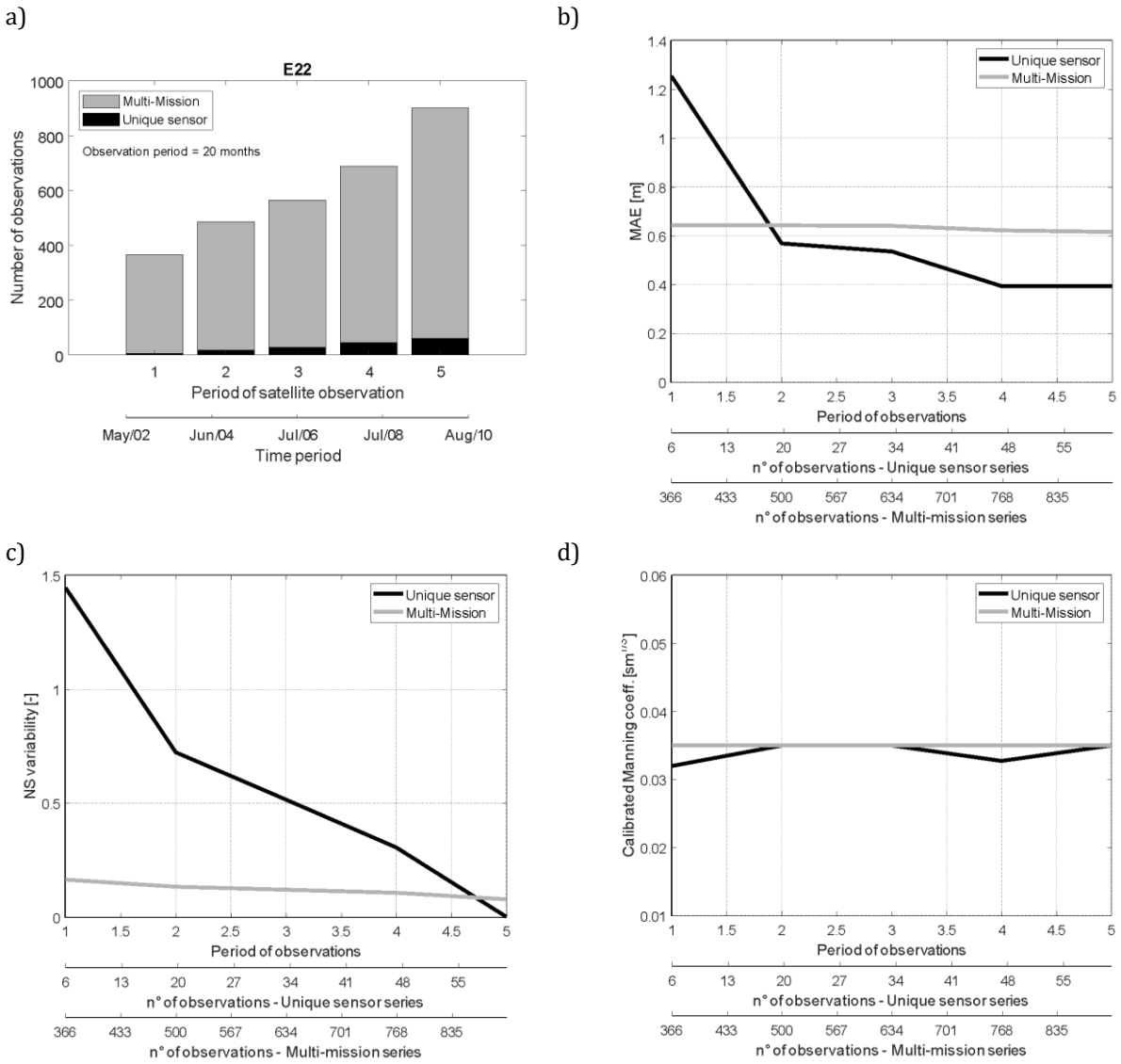


494 ***Figure 12***. *MM and E22: a) number of observations depending on the observation period; b) MAE, c) NS and d)*
495 *Manning's coefficient as a function of the number of available observations for unique sensor (black line)*
496 *and MM series (grey line).*
497
498

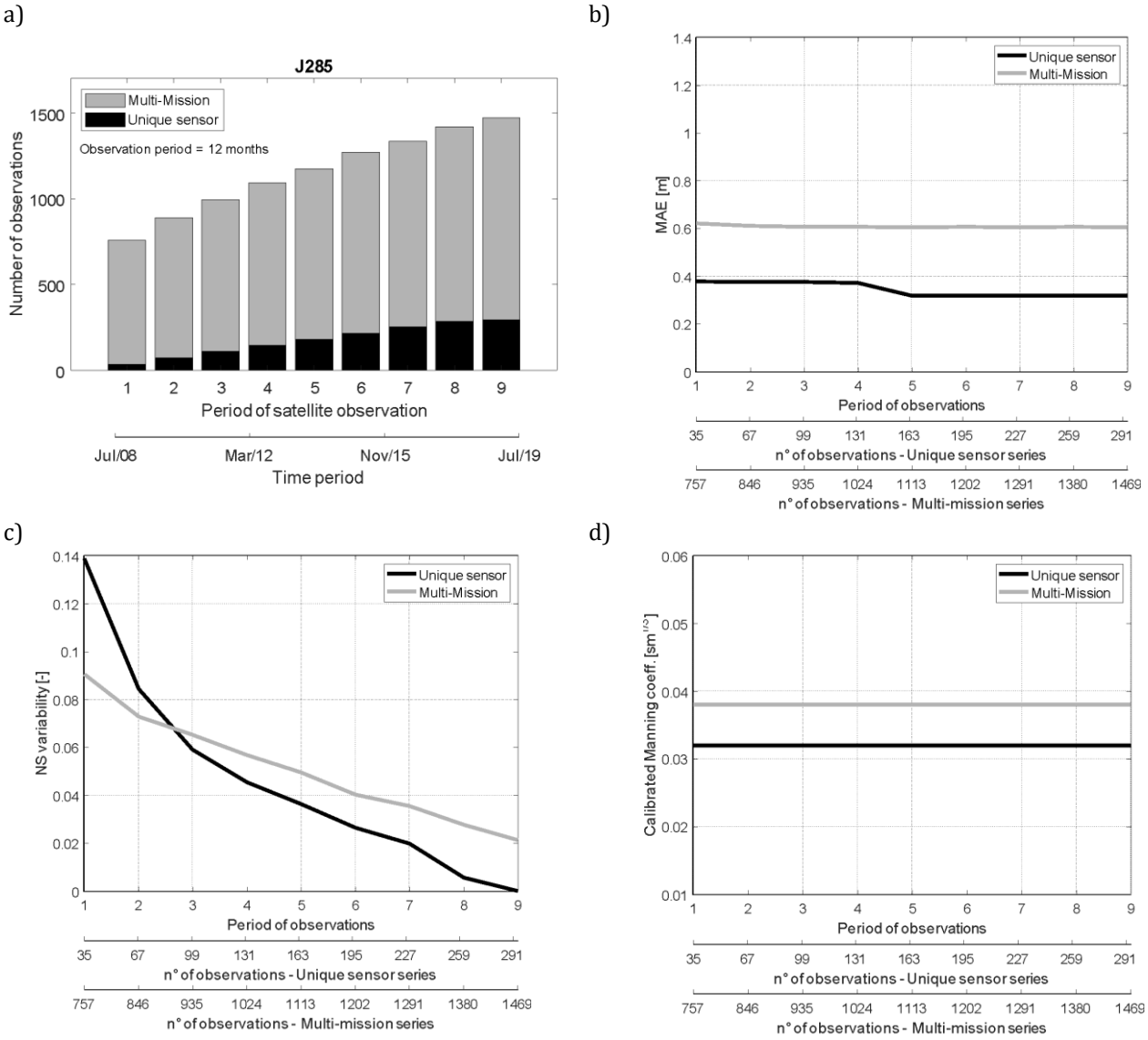


***Figure 13***. *MM and J2-85: a) number of observations depending on the observation period; b) MAE, c) NS and d) Manning's coefficient as a function of the number of available observations for unique sensor (black line) and MM series (grey line).*

504

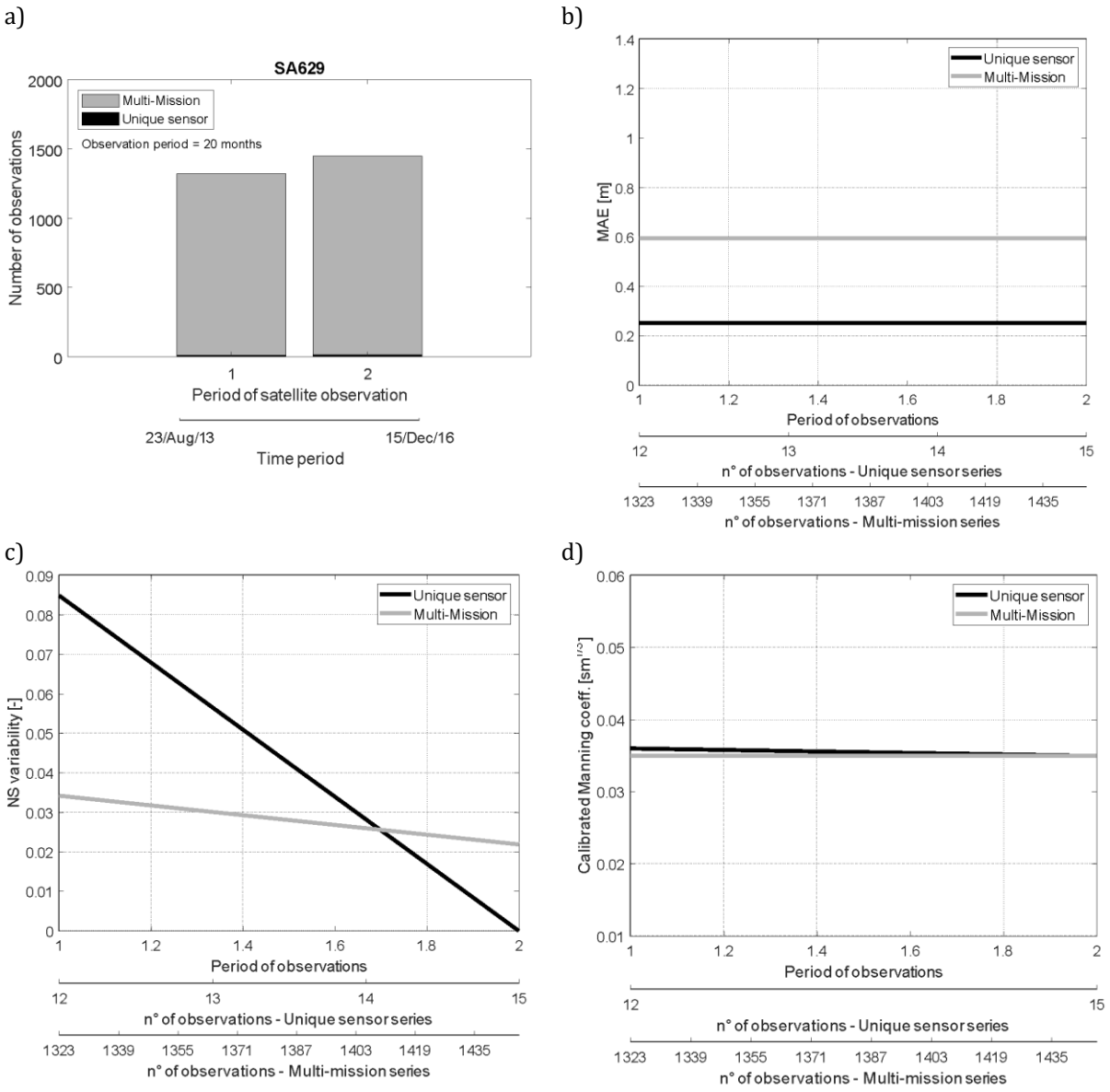


505

506 ***Figure 14***. *MM and SA629: a) number of observations depending on the observation period; b) MAE, c) NS and d)*
507 *Manning's coefficient as a function of the number of available observations for unique sensor (black line)*
508 *and MM series (grey line).*

509

510

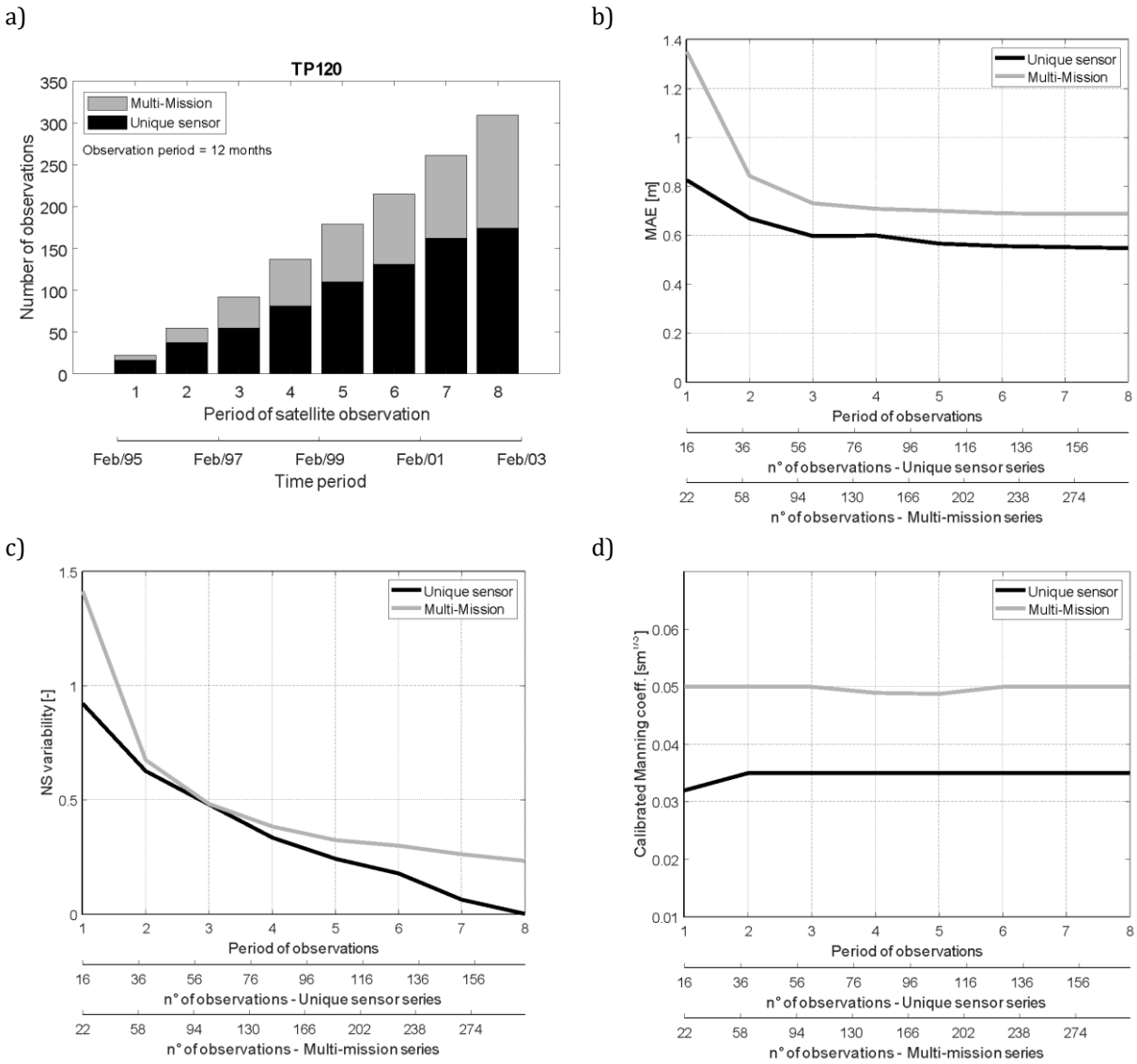


511
512 ***Figure 15***. *MM and TP120: a) number of observations depending on the observation period; b) MAE, c) NS and d)*
513 *Manning's coefficient as a function of the number of available observations for unique sensor (black line)*
514 *and MM series (grey line).*

515

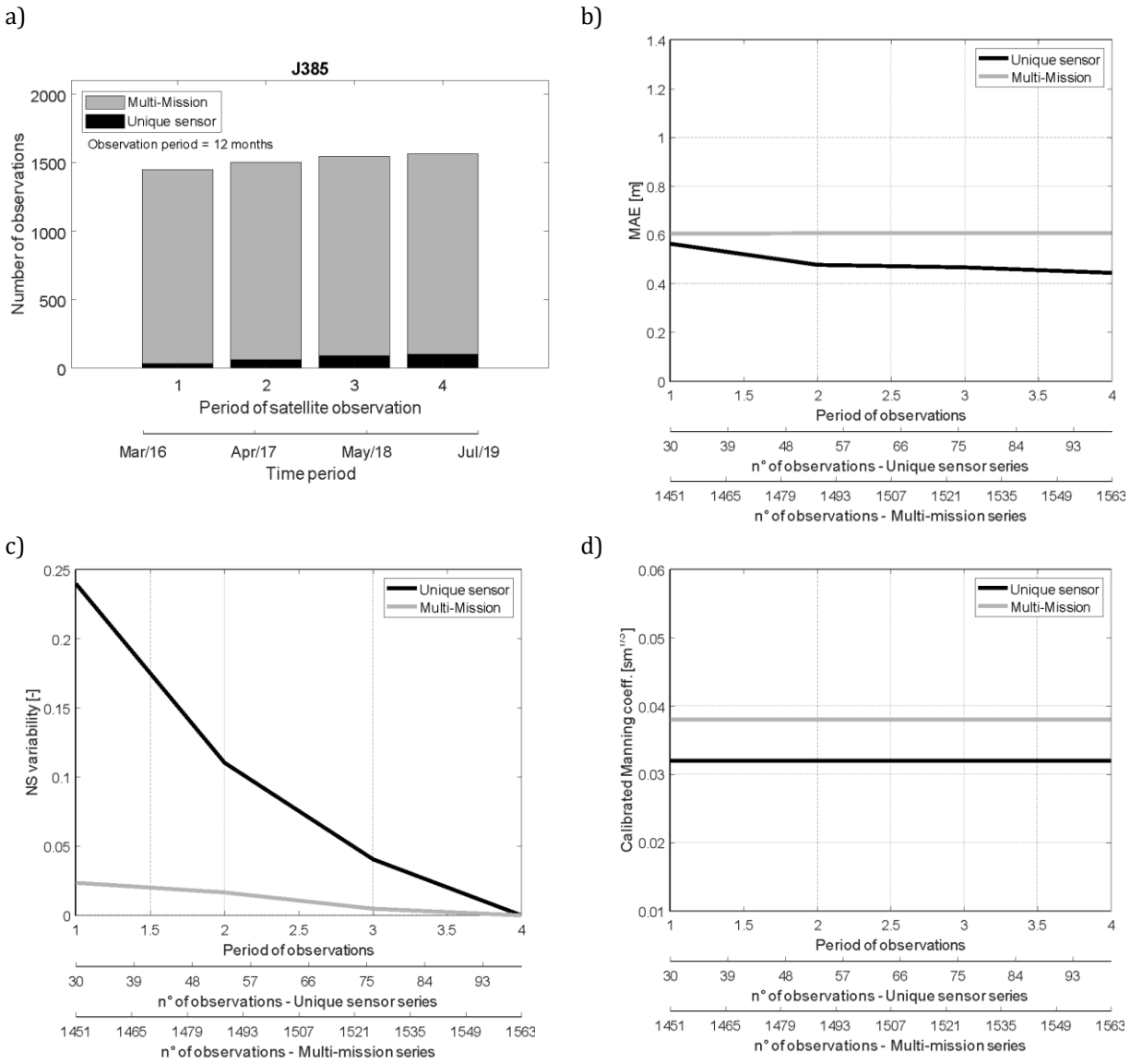


***Figure 16***. *MM and J3-85: a) number of observations depending on the observation period; b) MAE, c) NS and d) Manning's coefficient as a function of the number of available observations for unique sensor (black line) and MM series (grey line).*

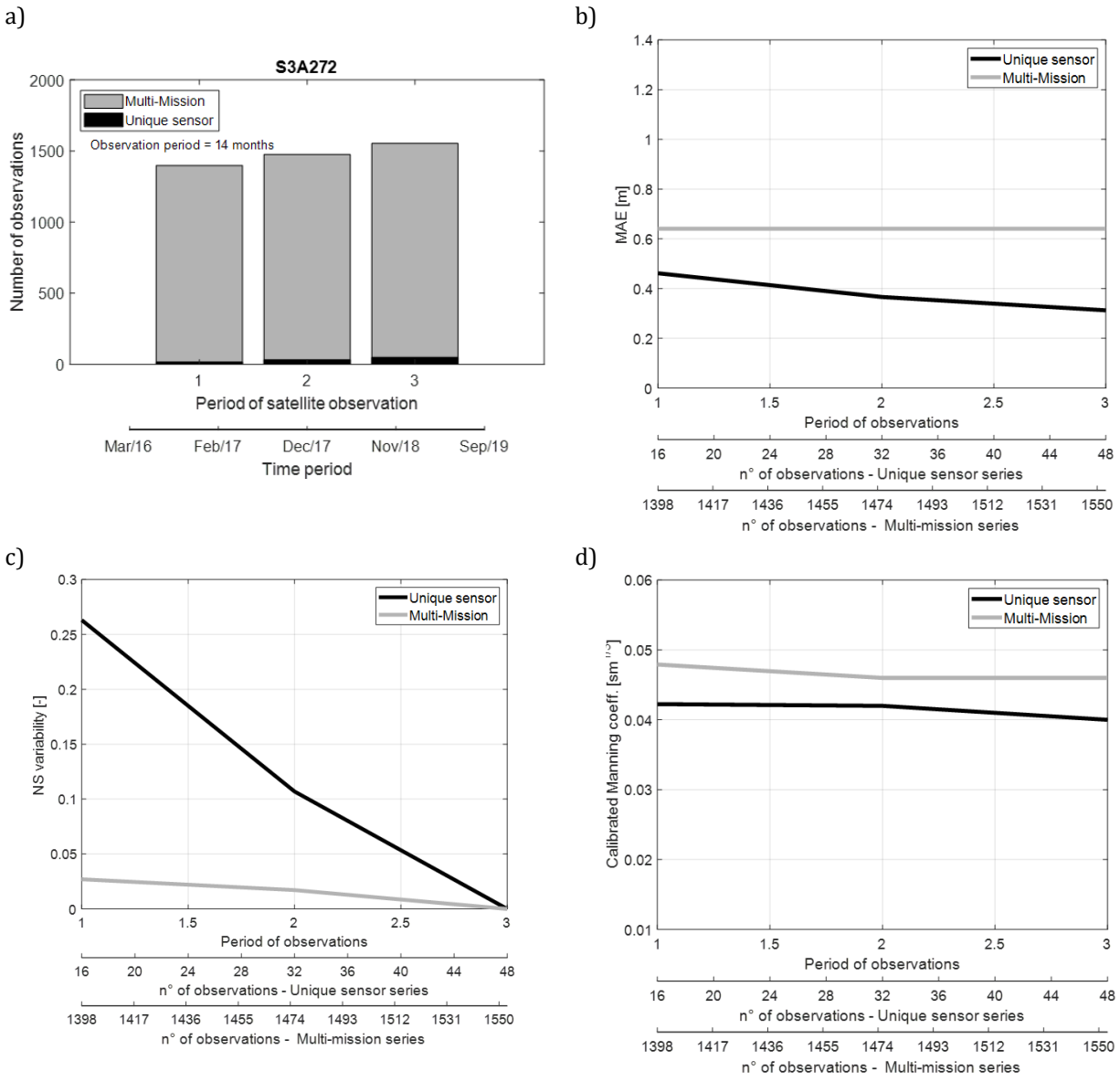


521 ***Figure 17****. MM and S3A-272: a) number of observations depending on the observation period; b) MAE, c) NS and d)*
522 *Manning's coefficient as a function of the number of available observations for unique sensor (black line)*
523 *and MM series (grey line).*
524
525
526
527

528 # 4 DISCUSSION

529 ## 4.1 Accuracy of altimetry products

530 Table 2 summarizes the comparison between satellite and original altimetry data. Excluding EX775, which
531 has a very limited number of observations, all the altimetry series show quite high R values, which are always
532 larger than 0.6 and generally improves moving from historical missions to the most recent ones. Similarly, NS
533 values are in general positive, with the few exceptions of EX775 and TP85. In general, J2 series outperform
534 all other missions providing a mean error, μ, of about 20 cm and the lowest values of standard deviation (μ =

0.38 cm in the worst case). Despite the limited amount of observations, S3B is the only time series having a lower mean error ($\mu = 0$), while S3A series show performance in line with those of J2 and S3B, unless irregular among the available VSs. J3 provides $\mu$ values comparable to those of J2, but higher standard deviations, $\sigma$. A possible justification can be due to the characteristics of J3 series, which appear shorter than those of J2 (nearly 1/3 in length; see Table 2) and characterized by a higher frequency of low-flow conditions. This latter aspect is evident in Figure 3, where J3 covers a period of time (2016-on) during which water levels are on average lower (meaning low flow period) than what observed by J2 (yellow lines). This aspect may play a significant role when considering possible hooking effect (or "off-nadir" effect, Schwatke *et al*., 2015), which is expected to be more relevant in case of smaller water extent. In addition to this, after a closer look at J3 data and correspondent observed level, the performance of J3 at VS 120 appears strongly influenced by few significant errors observed during a short period (beginning of 2018), during which the altimeter sensed water level considerably higher than the observed ones. Those errors, since the limited extent of J3 series, heavily affect the statistics, which would have been in line with those of J2 otherwise.

SA series ensure high correlation values, while MAE values are worse than those from the older mission E. This might be due to the limited length of the series (8 and 15 observations in total at the two available VSs). In contrast, despite the number of available observations, TP provides the worst results, with low NS and high MAE values. The mean error values, $\mu$, indicate a general overestimation of the satellite series ($\mu > 0$) with the only exception of TP120 that shows a negative bias. Finally, referring to ERS-2 data, Domeneghetti *et al*. (2015a) identify MAE values in the order of 0.7 m, with $\mu$ and $\sigma$ up to 0.64 cm and 0.84 cm, respectively, at two VS along the Po river.

Table 3 shows the results of the same comparison performed with MM series. Results highlight a uniform performance in terms of R (0.80). NS values are in general positive, even if always lower than 0.66. In general, performance indexes appear more homogeneous along the study area, which is somehow expected considering the way the MM series are defined along the river.

Looking at the spatial distribution of the error, the analysis performed does not enable the identification of a specific relationship among error magnitude and river morphology, such as river width or river orientation. However, it is worth noting that in general the performances obtained considering the MM series at a given location are always lower than those obtained considering the original altimetry series, with the only exception

563 of few VSs where the performances of the altimetry products were not convincing, perhaps due to their limited
564 length (e.g., VS 775). In such a case, MM series is more capable to reproduce the observed water level
565 dynamics.

566 **4.2 Values of satellite altimetry and effects of time series length on model calibration**

567 The results of the calibration performed using satellite altimetry shed some light on the potential of different
568 products for modelling applications. In particular, the influence of the number of observations on the variability
569 of the results varies in relation to the satellite product.

570 Assuming that a calibration result should be considered reliable when the variability of the roughness
571 coefficient is very limited (i.e., $\pm 0.005$ $s \cdot m^{-1/3}$ in terms of Manning's coefficient), this condition is reached in
572 case of considering a number of observations that varies from one mission to another. Looking at Figure 7,
573 this target is reached for E in case of using more than nearly 35 observations, which means nearly 3.5 years of
574 observation considering its revisit time (35 days). Similar results have been obtained considering ERS-2 series
575 (Domeneghetti *et al*., 2015a). The lengths of required series become smaller in case of TP (revisit time equal
576 to 10 days), which ensures reliable performance with 50 observations, recorded on average in 1.5 years. Better
577 performances are obtained in case of J2 series, for which the same performance is obtained calibrating the
578 model with nearly 30 observations (less than 1 year of record considering its temporal resolution). The same
579 number of observations is required by S3A, although its lower repeat period extends the time series up to more
580 than 2 years. Similarly, 30 observations are needed for J3-85, while nearly 60 (slightly more than 1.5 year) are
581 required for the J3-120. Again, this latter difference can be justified by the errors noticed for J3-120 series and
582 previously described. Regarding the satellite series EX, the limited number of available observations prevents
583 us from drawing general conclusions. The same holds for SA44 (8 measurements in total). Despite the limited
584 amount of data, the calibration results with S3B272 and SA629 are good: the calibration appears reliable
585 already with a limited number of data, nearly 10, which means a period of observation of approximately 1 year
586 and less than 1 year for SA and S3B, respectively, considering their repeat periods. In addition, this seems to
587 confirm the value of SA mission, which is the only one operating at Ka band among those considered. As a
588 matter of fact, although considering wider inland water bodies and rivers (e.g. nearly 5 km) Schwatke *et al*.,
589 (2015) proved the higher potential of a Ka-band instrument compared to the typical Ku-band sensors, thus
590 offering promising expectation from future satellite missions that envisage the adoption of Ka-band altimeter

(e.g. SWOT mission).

The evolution of the calibration performance in relation to *m*, number of observations, is clearly depicted by Figure 8, where the maximum MAE obtained during the calibrations typically decreases with extensive series. Looking at the errors obtained using in situ data (red lines), the maximum MAE reaches the minimum value after a limited amount of data, assuming errors that are almost uniform along the study area: the optimal error varies in the range ~10÷30 cm (see also Table 3). The evolution of the black lines (altimetry data) confirms previous findings on satellite potential. S3A, S3B, J3, J2 and TP products ensure the fastest achievement of the minimum error. However, regarding the distance between red and black lines, which can be considered as a measure of the error introduced in the model calibration when using altimetry data instead of in situ, E series provide performances comparable to that of J2 (see Table 4). On the contrary, TP series, despite being more frequent, introduce larger errors: nearly double that of E or J2.

Finally, it is worth highlighting the performance of S3B272, which ensures the lowest error among all considered satellite series. These results are clearly summarized in Figure 9, which shows the temporal distribution of the satellite series together with their calibration performances. What is evident is that, with the only exception of EX and caution on considering J3, the error and its variability are generally decreasing in time, showing a constant improvement in satellite capacity to remotely observe water elevation . This potential of altimetry time series is also confirmed by the validation results (Table 4), for which the lowest NS is equal to 0.54. In general, if not even better, NS values are comparable to the ones obtained during the calibration phase. Only in few cases the validation provided accuracy significantly worse than the one achieved during the calibration (e.g., S3B272, S3A272).

Findings concerning SARAL/Altika might be misleading since the poor performance at SA44, which is responsible for the significant size of the error box. As a matter of fact, the additional error introduced at SA629 is equal to 0.09 m, which is the lowest of all the series. Future analysis with longer SA series will reveal the real potential of this satellite product for model calibration.

Concerning the use of MM series on model calibration, in the light of the higher number of observations combined by MM series, the calibration easily converges to the final configuration (Figures 10 and 11). However, errors introduced using such series are higher than those associated with traditional series: Δ-RMSE and Δ-MAE are on average equal to 0.53 m and 0.38 m, respectively (Table 5). As expected, MM performances

619 in terms of model calibration do not vary from one location to another being the result of a spatial and temporal
620 combination of all available satellite dataset. However, it is also worth noting that using high frequency water
621 level series reduces the calibration accuracy (NS) also in case of referring to extended series of in situ data
622 (see comparison of NS values for in situ data in Tables 4 and 5). Since the calibration considers a constant
623 Manning's coefficient, we argue that this loss of efficiency might be due to the consideration of a higher
624 variability of river flow conditions, which include both low and peak flow regime. As a matter of fact, a model
625 calibrated referring to medium-to-large flow conditions, that are those most frequent in the river, might have
626 poor performance when used to reproduce low flow scenarios (see e.g. Moramarco e Singh, 2010;
627 Domeneghetti *et al*., 2012). Validation results confirm the potential of MM time series for model calibration,
628 reporting performances in line with those achieved calibrating the model using in situ data for the same time
629 period (values in brackets in Table 5).
630 Leaving aside specific performances of different single mission products, the calibrated roughness
631 coefficients obtained considering one time series at time (first two columns of Table 6) appear in line with
632 values obtained from previous studies performed over the study area, which shown a general decreasing trend
633 moving downstream (reference values are 0.004-0.042-0.025 $sm^{-1/3}$ for the upper, middle e lower river portion,
634 respectively; see Domeneghetti *et al*., 2014). Similar behaviour is also observed adopting MM series, with
635 variation on roughness values not particularly significant.

636 **4.3 Potential and limits of MM altimetry series for model calibration**

637 Using MM series always entails an additional error: Δ-RMSE and Δ-MAE are always positive, with values
638 up to 0.56 m and 0.38 m, respectively. The only exception is represented by MM-EX775, which is due to the
639 poor performance of EX series at that location. Thus, in case of considering the overall altimetry series length
640 ($m = L_{tot}$; which varies in relation to the series), the use of a single MM series for model calibration does not
641 provide benefits and is not recommended.
642 However, results presented in Figures 12-17 provide more insights: NS variability (panel *c)*) associated to MM
643 (grey lines) is always lower than the one obtained with the original series (black lines), thus providing more
644 stable calibration even for very short calibration periods. This is particularly significant in case of altimetry
645 series with limited observation frequency (i.e., 35 days, such as E and SA), for which the calibration
646 immediately converges to the real Manning coefficient (black and grey lines overlap in panels *d)*), even using

data observed within 1 observation period (i.e., 20 months; see e.g., Figure 12 and 14). On the contrary, differences are much larger and not negligible in case of satellite products characterized by higher temporal observation frequency (i.e., J2, J3 and TP). This might be explained by considering that, in case of high frequency series (i.e., those with revisit time of 10 days), the MM generation process further enhances the temporal coverage of the remote series, but it introduces errors larger than those associated with the original satellite series, which are still in any case frequent enough to provide a reliable calibration.

When using all MM series together, some differences emerged in terms of calibrated Manning's coefficients, which are not always in agreement with those obtained considering one VS at time (Table 6). This is due to the mutual interaction of the calibrating river cross-sections (VSs) that requires local modification of the friction values to deal with opposing biases. However, apart for few exceptions (MM120 and MMA272), the use of all MM series together provides performances along the entire river in line with those ensured by adopting one MM series at time, which is promising in assuring a proper simulation of flowing dynamics over long river stretch.

Although the improvement of the methodology used for the construction of MM series is out of the scope of the current investigation, a possible strategy towards an improvement of MM reliability and accuracy, at the expense of some temporal frequency reduction, could be the adoption of only best performing single missions (e.g., E, J2, J3 and SA). Preliminary trials on this matter did not provide satisfying results, but future work will further investigate in this direction. In this context, future analysis could also consider the opportunity to include other recent altimetry products that, although characterized by long repeat cycles, have high accuracy on water level measurement. This is the case for example of IceSat-2 (ATLAS altimetry; available from December 2018) that can ensure high accuracy on water elevation sensing but has a repeat period of 91 days (see e.g., Yuan *et al*., 2020). Shifting in space such information could further sustain satellite products exploitation for inland river monitoring. In addition, any progresses in the characterization of river geometry (e.g., river width) and of its dynamic (e.g., flow time lag), are expected to lead to further improvements in MM accuracy.

## 5 CONCLUSIONS

This study provides additional insights regarding the potential of satellite altimetry sensors for hydraulic

675 applications. Although not aspiring at providing an evaluation and comparison of altimetry missions in
676 absolute terms (a wider spectrum of rivers and flowing conditions would have been necessary), this work offers
677 a comprehensive and cross-missions view of the potential of such products, together with MM series, which
678 have been tested for hydraulic model calibration. To this end, we referred to a reach of nearly 140 km of the
679 Po river for which we implemented a quasi-2D hydraulic model based on detailed topography data.
680 In general, altimetry time series properly reproduce observed water level time series, showing correlation
681 coefficients (R) always larger than 0.6 in case of single missions. Despite limited to one VS, S3B (Sentinel-
682 3B) ensures the lowest error (ŋ=0). J2 (Jason 2) shows high accuracy (mean error equal to 20 cm), followed
683 by S3A (Sentinel-3A), J3 (Jason 3) and Envisat (E). Even though the limited extent of the derived time series,
684 SA (SARAL/Altika) shows promising performances with high R values (higher than 0.9). On the contrary and
685 despite the high number of observations, TP (TOPEX/Poseidon) series do not ensure reliable estimation of
686 water levels.
687 MM series ensures a uniform behaviour along the study area (R is nearly constant and equal to 0.80), however,
688 their performances at a given location are always lower than those obtained considering the original altimetry
689 series (see Tables 2 and 3).
690 Results of the model calibration depict a general temporal improvement of satellite performances moving from
691 the oldest to more recent missions, with the only exception of EX series (see Figure 9). The lower additional
692 error induced by the use of remote sensing data on model calibration (Δ-MAE) is limited to nearly 20 cm in
693 case of using J2 and E series, while it is larger (up to 30÷40 cm) in case of other series (up to 60 cm in case of
694 ERS-2 series; Domeneghetti *et al*., 2015a). J2 series ensure trustworthiness and reliability on the calibration
695 process with the lower temporal observation extent: lower than 1 year of data (~30 observations), followed by
696 J3 and S3A that reach the same reliability after 1.5, 1.6 and 2.2 years, respectively (i.e., 50, 60 and 30
697 observations, respectively). For a similar performance, E requires nearly 3.5 years of data (i.e, 35
698 observations). Using ERS-2 data would require a series extent up to 4.5 years (nearly 50 observations
699 considering a satellite revisit time of 35 days). Unless limited in time, results show SA and S3B time series
700 potential in achieving reliable calibration using only few observations (e.g., nearly 10).
701 The use of MM series for model calibration has provided errors higher than those obtained using original
702 satellite series in case of considering their overall length: additional errors are equal to 0.56 m and 0.38 m in

703 terms of Δ-RMSE and Δ-MAE, respectively.

704 However, the comparison of MM and original series' performances in relation to the number of available
705 observations depicts the potential of MM series, which are able to ensure calibrations more reliable than those
706 obtained in case of altimetry series provided by low frequency satellites (i.e., E, SA) that cover very short
707 period (e.g. 1÷2 observation period; 20-40 months). In these conditions MM series offer calibration
708 performances (i.e., reliable estimation of the friction coefficient and lower uncertainty) higher than those
709 ensured with the original series. However, if satellite sensors with higher temporal observation frequency are
710 available (i.e., J2 and J3), the use of original series, even though limited in terms of observations, appears to
711 be the best option. That said, MM series ensure a higher spatial coverage of the river, which could be significant
712 when referring to long river stretch and single altimetry missions characterized by long inter-track distances.

713

714 **6 ACKNOWLEDGEMENTS**

715 The authors are particularly grateful to the Interregional Agency for the Po River (Agenzia Interregionale per
716 il Fiume Po, AIPO, Italy) and Po River Basin Authority (Autorità di Bacino del Fiume Po, Italy) that allow the
717 access to the high resolution DTM of River Po. In situ hydrological data are available through hydrological
718 annual books and on line web service: DEXT3R - https://simc.arpae.it/dext3r/. The authors are grateful to the
719 European Space Agency for providing the ENVISAT data. The satellite data of TOPEX/Poseidon are provided
720 by Physical Oceanographic Distributed Active Archive Center (PODAAC)
721 ftp://podaacftp.jpl.nasa.gov/allData. Thanks are also due to AVISO (http://www.aviso.altimetry.fr) for
722 providing SARAL/ AltiKa data and Jason 2 hydrology product and Jason 3 data. SENTINEL-3A and
723 SENTINEL-3B series are extracted from the COPERNICUS data repository (https://scihub.copernicus.eu).

724

725

## 7 REFERENCE


Andreadis, K.M., Schumann, G.J., 2014. Estimating the impact of satellite observations on the predictability of large-scale hydraulic models. Adv. Water Resour. 73, 44–54. doi:10.1016/j.advwatres.2014.06.006

Aronica, G., Tucciarelli, T., Nasello, C., 1998. 2D Multilevel Model for Flood Wave Propagation in Flood-Affected Areas. J. Water Resour. Plan. Manag. 124, 210–217. doi:10.1061/(ASCE)0733-9496(1998)124:4(210)

Bates, P.D., Anderson, M.G., 1996. A preliminary investigation into the impact of initial conditions on flood inundation predictions using a time / space distributed sensitivity analysis. Catena 26, 115–134.

Barzaghi, R., Borghi, A., Carrion, D., Sona, G., 2007. Refining the estimate of the Italian quasi-geoid. Boll. di Geod. e Sci. Affin 66.

Biancamaria, S., Lettenmaier, D.P., Pavelsky, T.M., 2016. The SWOT Mission and Its Capabilities for Land Hydrology. Surveys in Geophysics 37 (2): 307–337 DOI: 10.1007/s10712-015-9346-y

Bjerklie, D. M., Dingman, S. L., Bolster, C. H., 2005. Comparison of constitutive flow resistance equations based on the Manning and Chezy equations applied to natural rivers. Water Resources Research, 41(11), 1–7. https://doi.org/10.1029/2004WR003776

Boergens, E., Nielsen, K., Andersen, O.B., Dettmering, D, S.F., 2017. River Levels Derived with CryoSat-2 SAR Data Classification — A Case Study in the Mekong River Basin. Remote Sens. 1–21. doi:10.3390/rs9121238

Bronstert, A., 2003. Floods and Climate Change : Interactions and Impacts 23.

Camorani, G., Cavazzini, A., Lombardo, G., Pappani, G., Forlani, G., 2006. Il rilievo altimetrico e batimetrico del Fiume Po nel tratto tra confluenza Ticino e l'incile, in: X Asita Nat. Conf. (in Italian).

Castellarin, A., Baldassarre, G.D.I., Brath, A., 2011. Floodplain management strategies for flood attenuation in the River Po. River Res. Appl. 27, 1037–1047. doi:10.1002/rra

Castellarin, A., Domeneghetti, A., Brath, A., 2011a. Identifying robust large-scale flood risk mitigation strategies: A quasi-2D hydraulic model as a tool for the Po river. Phys. Chem. Earth, Parts A/B/C 36, 299–308. doi:10.1016/j.pce.2011.02.008

Coss, S., Durand, M. T., Yi, Y., Jia, Y., Guo, Q., Tuozzolo, S., Shum, C. K., Allen, G. H., Calmant, S., & Pavelsky, T., 2020. Global River Radar Altimetry Time Series (GRRATS): new river elevation earth

754 science data records for the hydrologic community. Earth Syst. Sci. Data, 12(1), 137-150.
755 doi:10.5194/essd-12-137-2020
756 Cretaux, J. F., Berge-Nguyen, M., Calmant, S., Jamangulova, N., Satylkanov, R., Lyard, F., Perosanz, F.,
757 Verron, J., Montazem, A.S., Le Guilcher, G., Leroux, D., Barrie, J., Maisongrande, P., Bonnefond, P.,
758 2018. Absolute calibration or validation of the altimeters on the Sentinel-3A and the Jason-3 over Lake
759 Issykkul (Kyrgyzstan). Remote Sensing, 10(11), 1679.
760 Desai, S., 2018. Surface Water and Ocean Topography mission (SWOT), Science Requirements Document
761 (JPL document D-61923 Revision B, https://swot.jpl.nasa.gov/docs/D-
762 61923_SRD_Rev_B_20181113.pdf).
763 DHI, 2015. MIKE 11 - A Modelling System for Rivers and Channels - Reference Manual. Hørsholm,
764 Denmark.
765 Di Baldassarre, G., Montanari, A., 2009. Uncertainty in river discharge observations: a quantitative analysis.
766 Hydrol. Earth Syst. Sci. 13, 913–921. doi:10.5194/hess-13-913-2009
767 Domeneghetti, A., Castellarin, A., Brath, A., 2012. Assessing rating curve uncertainty and its effects on
768 hydraulic model calibration, Hydrol. Earth Syst. Sci., 16, 1191–1202, doi:10.5194/hess-16-1191-2012.
769 Domeneghetti, A., Tarpanelli, A., Brocca, L., Barbetta, S., Moramarco, T., Castellarin, A., Brath, A., 2014.
770 The use of remote sensing-derived water surface data for hydraulic model calibration. Remote Sens.
771 Environ. 149, 130–141. doi:10.1016/j.rse.2014.04.007
772 Domeneghetti, A., Carisi, F., Castellarin, A., Brath, A., 2015. Evolution of flood risk over large areas:
773 Quantitative assessment for the Po river. J. Hydrol. 527, 809–823. doi:10.1016/j.jhydrol.2015.05.043
774 Domeneghetti, A., Castellarin, A., Tarpanelli, A., Moramarco, T., 2015a. Investigating the uncertainty of
775 satellite altimetry product for hydrodynamic modelling. Hydrol. Process. 29, 4908–4918.
776 doi:10.1002/hyp.10507
777 Egido, A., Smith, W. H. ,2016. Fully focused SAR altimetry: theory and applications. IEEE Transactions on
778 Geoscience and Remote Sensing, 55(1), 392-406.
779 Frappart, F., Calmant, S., Cauhopé, M., Seyler, F., Cazenave, A., 2006. Preliminary results of ENVISAT RA-
780 2-derived water levels validation over the Amazon basin. Remote Sens. Environ. 100, 252–264.
781 https://doi.org/10.1016/j.rse.2005.10.027

Frasson, R. P. d. M., Schumann, G. J.-P., Kettner, A. J., Brakenridge, G. R., & Krajewski, W. F., 2019. Will the Surface Water and Ocean Topography (SWOT) Satellite Mission Observe Floods? Geophysical Research Letters. doi:10.1029/2019gl084686

Giustarini, L., Vernieuwe, H., Verwaeren, J., Chini, M., Hostache, R., Matgen, P., Verhoest, N.E.C., Baets, B. De, 2015. Accounting for image uncertainty in SAR-based flood mapping. Int. J. Appl. Earth Obs. Geoinf. 34, 70–77. doi:10.1016/j.jag.2014.06.017

Jiang, L., Madsen, H., Bauer-Gottwein, P., 2019. Simultaneous calibration of multiple hydrodynamic model parameters using satellite altimetry observations of water surface elevation in the Songhua River. Remote sensing of environment, 225, 229-247.

Kleinherenbrink, M., Naeije, M., Slobbe, C., Egido, A., Smith, W., 2020. The performance of CryoSat-2 fully-focussed SAR for inland water-level estimation. Remote Sensing of Environment, 237, 111589.

Loucks, D.P., van Beek, E., Stedinger, J.R., Dijkman, J.P.M., Villars, M.T., 2005. Water Resources Systems Planning and Management and Applications: An Introduction to Methods, Models and Applications, Unesco. doi:92-3-103998-9

Loughlin, F.E.O., Paiva, R.C.D., Durand, M., Alsdorf, D.E., Bates, P.D., 2016. A multi-sensor approach towards a global vegetation corrected SRTM DEM product. Remote Sens. Environ. 182, 49–59. doi:10.1016/j.rse.2016.04.018

Loughlin, F.O., Trigg, M.A., Schumann, G.J., Bates, P.D., 2013. Hydraulic characterization of the middle reach of the Congo River 49, 5059–5070. doi:10.1002/wrcr.20398

Luino, F., Cirio, C.G., Biddoccu, M., Agangi, A., 2009. Application of a model to the evaluation of flood damage 339–353. doi:10.1007/s10707-008-0070-3

Matgen, P., Hostache, R., Schumann, G., Pfister, L., Hoffmann, L., Savenije, H.H.G., 2011. Towards an automated SAR-based flood monitoring system : Lessons learned from two case studies. Phys. Chem. Earth 36, 241–252. doi:10.1016/j.pce.2010.12.009

Merz, B., Kreibich, H., Schwarze, R., Thieken, A., 2010. Assessment of economic flood damage. Nat. Hazards Earth Syst. Sci. 1697–1724. doi:10.5194/nhess-10-1697-2010

Montanari, A., Ceola, S., Baratti, E., Domeneghetti, A., Brath, A., 2017. Po River Basin, in: Singh, V.P. (Ed.), Handbook of Applied Hydrology, Second Edition. McGraw Hill, pp. 116-1/116-4.

Moramarco, T., Singh, V. P., 2010. Formulation of the entropy parameter based on hydraulic and geometric characteristics of river cross section, J. Hydrol. Eng.-ASCE, 15, 852–858.

Nash, J. E., Sutcliffe, J. V., 1970. River flow forecasting through conceptual models part I — A discussion of principles. Journal of Hydrology. 10 (3): 282–290. doi:10.1016/0022-1694(70)90255-6.

Neal, J., Schumann, G., Bates, P., 2012. A subgrid channel model for simulating river hydraulics and floodplain inundation over large and data sparse areas. Water Resour. Res. 48, 1–16. doi:10.1029/2012WR012514

Pappenberger, F., Beven, K., Horritt, M., Blazkova, S., 2005. Uncertainty in the calibration of effective roughness parameters in HEC-RAS using inundation and downstream level observations. J. Hydrol. 302, 46–69. doi:10.1016/j.jhydrol.2004.06.036

Schneider, R., Tarpanelli, A., Nielsen, K., Madsen, H., Bauer-gottwein, P., 2018. Evaluation of multi-mode CryoSat-2 altimetry data over the Po River against in situ data and a hydrodynamic model. Adv. Water Resour. 112, 17–26. doi:10.1016/j.advwatres.2017.11.027

Schwatke, C., Dettmering, D., Börgens, E., Bosch, W., 2015. Potential of SARAL / AltiKa for Inland Water Applications. Marine Geodesy 0419 (38): 626–643 DOI: 10.1080/01490419.2015.1008710

Silva, J.S. da, Calmant, S., Seyler, F., RotunnoFilho, O.C., Cochonneau, G., Mansur, W.J., 2010. Water levels in the Amazon basin derived from the ERS 2 and ENVISAT radar altimetry missions. Remote Sens. Environ. 114, 2160–2181. https://doi.org/10.1016/j.rse.2010.04.020

Garambois, P. A., Calmant, S., Roux, H., Paris, A., Monnier, J., Finaud-Guyot, P., Montazem, A.S., da Silva, J., 2017. Hydraulic visibility: Using satellite altimetry to parameterize a hydraulic model of an ungauged reach of a braided river. Hydrological Processes, 31(4), 756-767.

Tarpanelli, a., Brocca, L., Melone, F., Moramarco, T., 2013a. Hydraulic modelling calibration in small rivers by using coarse resolution synthetic aperture radar imagery. Hydrol. Process. 27, 1321–1330. doi:10.1002/hyp.9550

Tarpanelli, A., Barbetta, S., Brocca, L., Moramarco, T., 2013b. River discharge estimation by using altimetry data and simplified flood Routing modeling. Remote Sens. 5, 4145–4162. doi:10.3390/rs5094145

Tourian, M.J., Elmi, O., Chen, Q., Devaraju, B., Roohi, S., Sneeuw, N., 2015. A spaceborne multisensor approach to monitor the desiccation of Lake Urmia in Iran. Remote Sens. Environ. 156, 349–360.

doi:10.1016/j.rse.2014.10.006

Tourian, M.J., Elmi, O., Mohammadnejad, A., Sneeuw, N., 2017. Estimating River Depth from SWOT-Type Observables Obtained by Satellite Altimetry. Water 9, 1–22. doi:10.3390/w9100753

Tourian, M.J., Tarpanelli, A., Elmi, O., Qin, T., Brocca, L., Moramarco, T., Sneeuw, N., 2016. Spatiotemporal densification of river water level time series by multimission satellite altimetry. Water Resour. Res. 52, 1140–1159. doi:10.1002/2015WR017654

Vignudelli, S., Birol, F., Benveniste, J., Fu, L. L., Picot, N., Raynal, M., Roinard, H., 2019. Satellite altimetry measurements of sea level in the coastal zone. Surveys in Geophysics, 40(6), 1319-1349.

Yan, K., Tarpanelli, A., Balint, G., Moramarco, T., Baldassarre, G., 2014. Exploring the Potential of SRTM Topography and Radar Altimetry to Support Flood Propagation Modeling: Danube Case Study. J. Hydrol. Eng. 20. doi:10.1061/(ASCE)HE.1943-5584.0001018

Yuan, C., Gong, P., Bai, Y., 2020. Performance Assessment of ICESat-2 Laser Altimeter Data for Water-Level Measurement over Lakes and Reservoirs in China. Remote Sens., 12, 770.